https://doi.org/10.5194/egusphere-2026-3138
Preprint. Discussion started: 15 June 2026

Ammonia variability and trends from globally distributed FTIR measurements and model simulations

Beatriz Herrera[1,2,3], Enrico Dammers[3], Martine De Mazière[4], Omaira García[5], Michel Grutter[6], James W. Hannigan[7], Dylan B. A. Jones[2], Nicholas Jones[8], Emmanuel Mahieu[9], Maria Makarova[10], Kazuyuki Miyazaki[11], Isamu Morino[12], Isao Murata[13], Ivan Ortega[7], Mathias Palm[14], Anatoly Poberovskii[10], Takashi Sekiya[15], Dan Smale[16], Hannah Sill[17], Wolfgang Stremme[6], Ralf Sussmann[17], Geoffrey C. Toon[11], Corinne Vigouroux[4], Wei Wang[18], Tyler Wizenberg[3], and Kimberly Strong[2]

[1]Department of Physics, University of Toronto, Toronto, Ontario, Canada
[2]Department of Physical and Environmental Sciences, University of Toronto Scarborough, Toronto, Ontario, Canada
[3]Air Quality and Emissions Research (AER), Netherlands Organization for Applied Scientific Research (TNO), Utrecht, Netherlands
[4]Royal Belgian Institute for Space Aeronomy, Brussels, Belgium
[5]Izaña Atmospheric Research Centre, State Meteorological Agency of Spain (AEMET), Spain
[6]Instituto de Ciencias de la Atmósfera y Cambio Climático, Universidad Nacional Autónoma de México, Mexico City, Mexico
[7]Atmospheric Chemistry, Observations and Modeling, National Center for Atmospheric Research, Boulder, CO, USA
[8]School of Physics, Center for Atmospheric Chemistry, University of Wollongong, Wollongong, Australia
[9]Department of Astrophysics, Geophysics and Oceanography, UR SPHERES, University of Liège, Liège, Belgium
[10]Faculty of Physics, St. Petersburg State University, St. Petersburg, Russia
[11]Jet Propulsion Laboratory, California Institute of Technology, Pasadena, CA, USA
[12]National Institute for Environmental Studies (NIES), Tsukuba, Japan
[13]Graduate School of Environmental Studies, Tohoku University, Sendai, Japan
[14]Institut für Umweltphysik, University of Bremen, Bremen, Germany
[15]Japan Agency for Marine-Earth Science and Technology (JAMSTEC), Yokohama, Japan
[16]Earth Sciences New Zealand, Lauder, New Zealand
[17]Karlsruhe Institute of Technology, IMK-IFU, Garmisch-Partenkirchen, Germany
[18]Key Laboratory of Environmental Optics and Technology, Anhui Institute of Optics and Fine Mechanics, Hefei Institutes of Physical Science, Chinese Academy of Sciences, Hefei, China

Correspondence: Beatriz Herrera (beatriz.herrera@alumni.utoronto.ca)

Abstract. Ammonia (NH_3) is an important constituent in the global nitrogen cycle, present in both urban and remote environments. It is a source of reactive nitrogen and a precursor for particulate matter, thereby affecting atmospheric chemistry and radiative forcing. This work presents the seasonal and diurnal variability, along with long-term trends, of atmospheric NH_3 total columns retrieved from Fourier transform infrared (FTIR) spectroscopic solar absorption measurements at 22 ground-based sites, globally distributed from 45°S to 80°N. Comparisons are made with simulations from the GEOS-Chem High Performance (GCHP) chemical transport model and the Tropospheric Chemistry Reanalysis (TCR-2) NH_3 product. The mean NH_3 total columns from the FTIR time series ranged from 0.12×10^{15} to 19.20×10^{15} molecules cm^{-2}, with the smallest columns found at the Arctic and high-altitude sites, and the largest in urban areas. Significant enhancements were attributed to

https://doi.org/10.5194/egusphere-2026-3138
Preprint. Discussion started: 15 June 2026

biomass burning, and NH_3 emissions from volcanic eruptions were detected at the Izana site. The seasonal patterns are similar across most sites, with maxima mainly related to the volatilization of NH_3 due to higher temperatures. The diurnal variability differs significantly and depends on the characteristics of each site and local sources. Most sites have positive trends in the total column, with a mean value (and 95% confidence interval) for all sites of 3.82 (3.29–4.35)% for the FTIR measurements, 3.66 (3.35–3.97)% for GCHP, and 6.49 (2.00–10.98)% for TCR-2. GCHP exhibited a better general agreement with the FTIR observations than TCR-2; potential reasons for this are explored, including a sensitivity test on the emissions used.

1 Introduction

The nitrogen cycle has changed significantly since the introduction of the industrial fixation of nitrogen (Battye et al., 2017). With the growing world population and demand for food, fertilizer application has been increasing, especially since 1960 with the introduction of synthetic nitrogen fertilizers; it is estimated that currently, the anthropogenic flux of fixed or reactive nitrogen to the biosphere is roughly equivalent to the total flux from natural sources (Battye et al., 2017). Part of this nitrogen is lost to the environment in the form of emissions of nitrogen compounds, like ammonia (NH_3) (Paulot et al., 2014; Battye et al., 2017) for which emissions might reach 130 Tg NH_3-N yr^{-1} by 2100 (Sutton et al., 2013). Emissions of reduced N to the atmosphere are a key driver for atmospheric composition and chemistry in the twenty-first century (Fowler et al., 2013).

In the atmosphere, NH_3 is the most abundant alkaline compound. It is involved in several chemical reactions, such as the neutralization of atmospheric acidity and the formation of particulate matter, with strong consequences for the environment and human health (Behera et al., 2013). The main sources of NH_3 are related to agricultural activities (Sutton et al., 2008, 2013); for example, according to an estimate made by Paulot et al. (2014), out of the total global emissions of 54 Tg NH_3-N yr^{-1}, 34 Tg NH_3-N yr^{-1} come from manure and fertilizer applications, with the remainder related to other natural and anthropogenic sources such as open fires or industries. Once in the atmosphere, the primary chemical pathways are wet and dry deposition and conversion to particulate form (Behera et al., 2013; Sutton et al., 2013; Khan et al., 2020).

NH_3 emissions contribute significantly to $PM_{2.5}$ formation by its conversion to ammonium salts, which act as precursors and can account for up to 50% of particulate matter mass (Behera et al., 2013), a key factor in premature human mortality (Paulot et al., 2014; Giannakis et al., 2019). Despite the importance of atmospheric NH_3, most countries around the world do not have regulations to directly reduce NH_3 emissions, compared with the efforts to reduce NO_x and SO_2 emissions (Behera et al., 2013). Control of NO_x emissions contributed to the reduction in deposition of oxidized nitrogen (NO_y = the sum of all oxidized nitrogen species except N_2O). However, deposition of reduced nitrogen (NH_x) such as NH_3 increased (Tan et al., 2020). In addition, future increases in emissions are expected due to the potential use of NH_3 as a hydrogen carrier for the production of renewable energy, specifically using industrially-produced NH_3 with no or almost no carbon dioxide (green ammonia) for which production has increased in popularity in recent years (Olabi et al., 2023).

NH_3 has a short lifetime in the atmosphere, on the order of hours to a few days (Dammers et al., 2016, 2019; Nair and Yu, 2020; Evangeliou et al., 2021). NH_3 emissions and deposition strongly depend on environmental conditions; temperature and moisture play a crucial role in determining NH_3 concentrations on diurnal to annual scales (Sutton et al., 2013). NH_3 exhibits

https://doi.org/10.5194/egusphere-2026-3138
Preprint. Discussion started: 15 June 2026

a strong temporal and spatial variability that ranges over three orders of magnitude near the surface (Shephard et al., 2011). Previous studies, mainly using satellite observations, have shown a clear NH_3 seasonal cycle with temperature dependence in several sites around the world, with the seasonality driven by management differences and peaks during fertilizer of manure applications where applicable, and the interannual variability is attributed to meteorological conditions and agricultural constraints (Sutton et al., 2013; Paulot et al., 2014; Viatte et al., 2020).

Van Damme et al. (2015) used satellite data to show the worldwide spatiotemporal variability of atmospheric NH_3 using morning and evening measurements by the Infrared Atmospheric Sounding Interferometer (IASI) between 2008 and 2013. For most regions, defined seasonal cycles were reported, with the greatest concentrations found in Asia. The NH_3 columns vary widely around the world. For example, for Central America, the highest columns were during April and March and for South America during September and October, while Europe and North America showed higher columns during the spring season with columns around $1.5 - 2 \times 10^{16}$ molec. cm^{-2}. However, IASI measurements tend to underestimate NH_3 total columns compared to ground-based FTIR data (Dammers et al., 2016), and with limited measurements (Van Damme et al., 2015), it is not possible to determine the diurnal variability. In addition, NH_3 from biomass burning emissions contributes to seasonal variability over certain regions, for example, Central South America, as described by Whitburn et al. (2015), where the interannual variability of Fire Radiative Power (FRP) represented the intensity of NH_3 and CO enhancements from fire events between August and October.

Previous studies have investigated NH_3 trends in different regions using satellite or ground-based data. In North America, using surface data from monitoring stations distributed across Canadian and American urban, rural, and remote sites, positive trends in NH_3 mixing ratios between 20% and 50% from 2008 to 2015 at urban and agricultural sites were reported, mainly attributed to changes in the NH_3 - NH_4^+ partitioning (Yao and Zhang, 2016). In addition, more recent positive trends in reduced N in the USA have also been reported by Benish et al. (2022). More studies such as Yamanouchi et al. (2021) and Herrera et al. (2022) explored NH_3 over Toronto and Mexico City respectively using solar Fourier transform infrared spectroscopy (FTIR), also finding positive trends. In China, Chen et al. (2023) reported that according to several inventories NH_3 emissions from different anthropogenic sectors have doubled since 1980. In terms of global approaches, Van Damme et al. (2021) used ten years of global satellite data to derive trends of NH_3 total columns, reporting a worldwide increase of $12.8 \pm 1.3\%$ between 2008 and 2018, with increases over east Asia, western and central Africa, western and southern Europe, and North America; mainly attributed to anthropogenic factors affecting the lifetime of atmospheric NH_3. Warner et al. (2017) reported positive trends of NH_3 over several major agricultural areas around the world, with drivers mainly related to changes in fertilizers use, control of sulphur and nitrogen oxide emissions, and increasing temperatures.

This work uses NH_3 total columns from ground-based FTIR measurements, and NH_3 simulations, from the the GEOS-Chem High Performance (GCHP) global chemical transport model (CTM) and the Tropospheric Chemistry Reanalysis product (TCR-2), to examine the variability and trends of atmospheric NH_3 at 22 sites globally distributed, in particular the diurnal variability that has been poorly explored in previous studies. The paper is organized as follows. Section 2 describes the datasets and methods, starting with the FTIR site characteristics and retrieval strategy, followed by the model, reanalysis product, and trend analysis equations. Section 3 presents the FTIR measurements and the variabilities and trends. Section 4 describes

https://doi.org/10.5194/egusphere-2026-3138
Preprint. Discussion started: 15 June 2026

the comparison between the FTIR and modeled NH_3 products at each site. Finally, Section 5 summarizes the most relevant conclusions of this work.

2 Datasets and Methods

2.1 Ground-based FTIR NH_3 Measurements

2.1.1 FTIR Sites

Most of the sites included in this study are affiliated with the Network for the Detection of Atmospheric Composition Change (NDACC) (De Mazière et al., 2018), contributing data from high-resolution FTIR spectrometers. Most sites use the Bruker Optik GmbH IFS 120/125 HR spectrometer and record solar absorption spectra with a typical spectral resolution of 0.0035 cm^{-1}, equipped with either KBr or CaF_2 beamsplitters, and HgCdTe and InSb detectors, with three exceptions. The Toronto instrument is a high resolution ABB Bomen DA8, that has been providing measurements since mid-2002. The Mexico City instrument is a low-resolution Bruker Optik GmbH Vertex 80, which was included in this study due to the relevance of the site, as it is located in the south of Mexico City, one of the largest metropolitan areas in the world, and the largest in North America. The Los Angeles instrument is the MkIV high-resolution FTIR spectrometer, which has been performing ground-based observations since the 1980s, mainly in California (Toon, 1991; Sen et al., 1996; Toon et al., 2018).

Table 1 presents the main characteristics of each of the 22 FTIR sites. The primary NH_3 sources are based on the emissions inventories used for the GCHP simulations (described in Section 2.2.1) and are sorted by their contribution relevance for each site. Eureka, Thule, and Ny Alesund are Arctic sites where NH_3 sources are limited. Zugspitze, Jungfraujoch, Izana, Altzomoni, and Reunion Maido are high-altitude stations, with generally smaller NH_3 columns. St. Petersburg, Toronto, Los Angeles, Hefei, and Mexico City are sites located in heavily urban areas with populations of millions. Bremen, Boulder, Tsukuba, Paramaribo, Porto Velho and Wollongong are located in less urbanized areas, while Garmisch, Reunion St. Denis, and Lauder are more remote sites. Data from the NDACC FTIR instruments have been used to accurately document trends of many stratospheric and tropospheric gases (De Mazière et al., 2018).

2.1.2 FTIR NH_3 Retrieval Strategy

The retrieved NH_3 total columns presented in this work were mainly obtained following the strategy recommended in Dammers et al. (2015), which is briefly described in the following paragraph. For most sites, the solar FTIR spectra were analyzed using the SFIT4 retrieval algorithm (https://wiki.ucar.edu/display/sfit4/) version 0.9.4.4 to obtain the NH_3 total columns, except for Garmisch, Zugspitze and Izana, which used PROFFIT9 (Hase et al., 2004), and Los Angeles which used GFIT (Roche et al., 2021; Zeng et al., 2021; Laughner et al., 2024).

The SFIT4 retrieval uses two microwindows (MW) both in the ν_2 vibrational band of NH_3: MW1 (930.32 to 931.32 cm^{-1}) and MW2 (966.97 to 967.675 cm^{-1}). For some sites, wider MW1 (929.40 to 931.4 cm^{-1}) and MW2 (962.10 to 970.0 cm^{-1}) or a third MW in between them (MW3, 950.2 to 952.0 cm^{-1}) were used, especially for sites with small ambient NH_3 concentra-

https://doi.org/10.5194/egusphere-2026-3138
Preprint. Discussion started: 15 June 2026

Table 1. FTIR sites used in this study. The primary NH_3 sources are from the emissions inventories used in the GCHP simmulations.

Station	Latitude	Longitude	Elevation m.a.s.l.	Measurement Period	Primary NH_3 Sources
Eureka	80.05°N	86.4°2W	610	2006–2020	Anthropogenic, natural, biomass burning, seabirds
Ny Alesund	78.92°N	11.93°E	20	2017–2019	Natural
Thule	76.53°N	68.74°W	225	1999–2022	Seabirds, biomass burning
St. Petersburg	59.90°N	29.80°E	20	2010–2022	Anthropogenic, natural, biomass burning
Bremen	53.10°N	8.80°E	27	2004–2018	Anthropogenic, natural
Garmisch	47.48°N	11.06°E	743	2004–2007	Anthropogenic, natural
Zugspitze	47.42°N	10.98°E	2694	1995–2023	Anthropogenic, natural
Jungfraujoch	46.55°N	7.98°E	3580	2008–2023	Anthropogenic, natural, biomass burning
Toronto	43.66°N	79.40°W	174	2002–2023	Anthropogenic, natural, biomass burning
Boulder	39.99°N	105.26°W	1634	2010–2022	Anthropogenic, natural, biomass burning
Tsukuba	36.05°N	140.13°E	31	2014–2022	Anthropogenic, natural, biomass burning
Los Angeles	34.20°N	118.17°W	345	1985–2024	Anthropogenic, natural, biomass burning
Hefei	31.90°N	117.17°E	30	2017–2022	Anthropogenic, natural, biomass burning
Izana	28.30°N	16.48°W	2367	2000–2022	Anthropogenic, natural, biomass burning
Mexico City	19.32°N	99.17°W	2280	2012–2022	Anthropogenic, natural, biomass burning
Altzomoni	19.11°N	98.65°W	3985	2012–2022	Anthropogenic, natural, biomass burning
Paramaribo	5.81°N	55.21°W	23	2018–2019	Natural, anthropogenic, biomass burning
Porto Velho	8.77°S	63.87°W	87	2019	Biomass burning, anthropogenic, natural
Reunion St. Denis	20.90°S	55.50°E	85	2004–2011	Anthropogenic, natural
Reunion Maido	21.10°S	55.40°E	2155	2013–2023	Anthropogenic, natural
Wollongong	34.41°S	150.88°E	30	2007–2022	Anthropogenic, natural, biomass burning
Lauder	45.04°S	169.68°W	370	1996–2022	Anthropogenic, natural, biomass burning

tions. The retrievals included the interfering species H_2O, CO_2, O_3, CO, HNO_3 and N_2O for all stations, and temperature and pressure profiles obtained from the USA National Centers for Environmental Prediction (NCEP). Spectroscopic parameters were obtained from the high-resolution transmission molecular absorption database HITRAN 2008 (Rothman et al., 2009), except for St. Petersburg, which used HITRAN 2012 (Rothman et al., 2013). The a priori profiles for the interfering gas were obtained from 40-year averages of simulations from the Whole Atmosphere Community Climate Model (WACCM) (Eyring et al., 2007; Marsh et al., 2013). For NH_3, the profiles from WACCM are only representative of remote regions; for this reason most of the sites used scaled a priori profiles derived from five years of averaged NH_3 simulations from the global chemical transport model GEOS-Chem v11. Constructed and scaled a priori profiles from GEOS-Chem simulations have been used previously for the retrieval of trace gases with good results (Shephard et al., 2011; Shephard and Cady-Pereira, 2015; Bader et al., 2017; Herrera et al., 2022), and scale factors are empirically calculated based on the convergence of the retrieval. The

https://doi.org/10.5194/egusphere-2026-3138
Preprint. Discussion started: 15 June 2026

average degrees of freedom for signal (DOFS) for all sites was 1.07 ± 0.15, indicating that the retrieval contains approximately one independent piece of information. The total error on the NH_3 total columns was calculated as the square root sum of the squares of all systematic and statistical errors (García et al., 2021), ranging between 0.1 and 2.0 with an average value for all sites of $0.93 \pm 1.30 \times 10^{15}$ molec. cm^{-2}.

2.2 Simulations of NH_3

2.2.1 GEOS-Chem

GEOS-Chem is a global 3-D model CTM (http://geos-chem.org) that is driven by assimilated meteorological fields from the NASA Global Modeling and Assimilation Office (GMAO). For this work, the high-performance version of GEOS-Chem was employed (Eastham et al., 2018; Martin et al., 2022). This version of GEOS-Chem runs on the native Goddard Earth Observing System cubed-sphere model grid. The analysis here uses the GCHP version 14.1.1 simulation from 2003 to 2021 driven by Modern-Era Retrospective Analysis for Research and Applications, version 2 (MERRA-2) (Gelaro et al., 2017), meteorological fields at C48 resolution, which is comparable to a resolution of $2^\circ \times 2.5^\circ$ (Bindle et al., 2021). The vertical resolution of the model consists of 72 levels from the surface to 0.01 hPa (approximately 80 km). Anthropogenic emissions are from the Community Emissions Data System (CEDS) v2 (Hoesly et al., 2018), biomass burning emissions from the Global Fire Assimilation System (GFAS) (Kaiser et al., 2012) v1.2, and natural emissions from the Global Emissions Inventory Activity (GEIA) (Graedel et al., 1993).

The analysis presented here uses a full-chemistry simulation that covers the period from 1 January 2003 to 31 December 2021. The model spin-up was performed for the full year of 2002 to provide the initial conditions for the simulation. The model transport and chemical operator time steps were selected for 10 and 20 minutes, respectively, as recommended by Philip et al. (2016) to minimize simulation errors. The modeled fields were archived at a temporal resolution of two hours for comparison with the FTIR observations. More details and applications of this long-term GCHP simulation can be found in Wizenberg et al. (2024). In addition to the 2003-2021 GCHP run, a one-month simulation was performed to explore the effect of changing the global emissions, by using the Hemispheric Transport of Air Pollution (HTAP) v3 emissions (Janssens-Maenhout et al., 2015), instead of CEDSv2, maintaining the same model configuration. The results of this simulation are discussed in Section 4.3.

2.2.2 TCR-2

The Tropospheric Chemical Reanalysis product (Miyazaki et al., 2020a) is a reanalysis product that consists of a global CTM and a data assimilation technique to optimize chemical concentrations and emissions of various chemical species. The TCR-2 ozone product is very well known and has been compared with several ozone reanalysis products, showing improved agreement with independent ground and ozone-sonde observations (Huijnen et al., 2020). In this work, the TCR-2 NH_3 product was evaluated. The reanalysis was produced using the MIROC-CHASER CTM (Watanabe et al., 2011) and an ensemble Kalman filter (EnKF) within the Multi-mOdel Multi-cOnstituent Chemical data assimilation (MOMO-Chem) (Miyazaki et al., 2020b) to assimilate observations of O_3, CO, NO_2, HNO_3 and SO_2 from multiple satellite instruments. The data assimilation system

https://doi.org/10.5194/egusphere-2026-3138
Preprint. Discussion started: 15 June 2026

simultaneously updates tropospheric emissions and chemical concentrations of 35 chemical species described in Miyazaki et al. (2012, 2015, 2020a). The representation of tropospheric chemistry, including NO_x and SO_2 emissions, is improved by assimilating NO_2 measurements from the Ozone Monitoring Instrument (OMI), the Global Ozone Monitoring Experiment (GOME-2), and the Scanning Imaging Absorption Spectrometer for Atmospheric Cartography (SCIAMACHY), and SO_2 from OMI.

Although NH_3 measurements were not directly assimilated in this product, the assimilation of NO_x and SO_2 can influence the NH_3 analysis. For instance, an analysis of the COVID-19 lockdown period showed that while NO_x and SO_2 emission reductions directly decreased nitrate and sulfate aerosols, they also led to a decrease in ammonium aerosols, even though NH_3 emissions remained unchanged in this analysis. This effect can be attributed to changes in NH_3 lifetime (Sekiya et al., 2023).

The TCR-2 product used in this work has a horizontal resolution of $1.1^\circ \times 1.1^\circ$ and consists of 32 vertical levels from the surface to 4.4 hPa. The TCR-2 fields were archived at a temporal resolution of 2 hours between 2005 and 2018. A priori anthropogenic emissions used in the reanalysis are from the HTAPv2 emissions (Janssens-Maenhout et al., 2015), biomass burning emissions from GFED v4 (Randerson et al., 2017), and soil emissions from GEIA (Graedel et al., 1993). The HTAP emission inventory has a $0.1^\circ \times 0.1^\circ$ resolution between 2000 and 2018 and is used to study trends and transport of air pollutants.

2.3 Trend Analysis

To derive long-term trends for the time series, we used a linear trend model with fitted Fourier series to account for seasonality, and bootstrap resampling methods to derive the 95% confidence intervals following the methodology of Friedrich et al. (2020). The trend model is described as follows:

$$y_t = d_t + s_t + u_t \tag{1}$$

where y_t are NH_3 measurements at time t, d_t is the unknown trend, s_t is the intra-annual seasonal pattern, and u_t is the error term. s_t is described by Fourier terms given by Equation 2.

$$s_t = \sum_{j=1}^{S} a_j cos(2j\pi t) + b_j sin(2j\pi t) \tag{2}$$

where a_j and b_j are the Fourier series parameters.

The seasonal variability is relevant for trends in atmospheric gases, and previous studies have shown that this variability is well captured by using the Fourier series of order 3 (S=3) (Gardiner et al., 2008; Franco et al., 2016; Prignon et al., 2019; Yamanouchi et al., 2021; Friedrich et al., 2020; Wizenberg et al., 2024). For this study, we apply Fourier series fitting of S=3 to the daily means of the NH_3 total column time-series data from the FTIR sites, GCHP, and TCR-2, to sites with more than 150 data points to ensure a good fit of the linear trend model. In addition, to estimate the uncertainty, we used bootstrap resampling methods, with a bootstrap population of 5000 as recommended in Gardiner et al. (2008), and an autoregressive wild bootstrap method (AWB) as recommended by Friedrich et al. (2020) to obtain the corresponding 95% confidence intervals (CI). The latter is more suitable for analyzing geophysical time series as it is specifically designed to account for missing observations,

https://doi.org/10.5194/egusphere-2026-3138
Preprint. Discussion started: 15 June 2026

auto-correlation, and seasonal effects in the datasets. Trends for which the CI does not include zero are considered statistically significant.

3 FTIR Results

3.1 Time Series

The retrieved total column time series of NH_3 from the 22 FTIR sites are shown in Figure 1. The NH_3 time series are very diverse across all sites, with Thule, Zugspitze, Toronto, Los Angeles, Izana, and Lauder, the only sites with more than 20 years of data. Most of the sites have between ten and 20 years of data, and only five sites have less than three years of data. The largest total columns of NH_3 are seen in Hefei, Bremen, Toronto, Mexico City and Porto Velho. These sites are in urban areas influenced by nearby agricultural activities, local sources, and biomass burning events. In contrast, the smallest total columns of NH_3 are mainly at the Arctic sites, where the NH_3 sources are limited, and in Reunion Maido and Jungfraujoch, two high-altitude sites that most likely were measuring NH_3 background concentrations.

However, noticeable enhancements can be observed at some of the sites, such as Eureka, Thule, Izana, Los Angeles, Mexico City, Altzomoni, Paramaribo, Porto Velho and Reunion Maido, mainly attributed to biomass burning events. The NH_3 enhancements at Eureka and Thule were linked to the 2017 Canadian wildfires by Lutsch et al. (2019). A large fire that occurred in the Amazon that reached several regions, analyzed by Bencherif et al. (2020), potentially reached Porto Velho and Paramaribo in August 2019. The NH_3 enhancements in late 2019 at the Reunion Maido site could be from biomass burning plumes from Africa and even the Amazon region (Callewaert et al., 2022).

Simultaneous enhancements of NH_3 and CO at Porto Velho and Reunion Maido during 2019 are shown in Figures A1 and A2 in the Appendix, as CO is largely emitted by fires: it has a longer lifetime than NH_3 and can be used as a reference species (Whitburn et al., 2017). For Mexico City, the simultaneous enhancements of NH_3 and CO are shown in Figure A4 during May 2019; this enhancement was part of a pollution event further discussed in Rios et al. (2023). Unfortunately, there are no simultaneous measurements of CO at Altzomoni during the enhancement observed in late March 2019; however, a few fires in the surrounding areas were detected by the Aqua-MODIS instrument (https://wvs.earthdata.nasa.gov). Similarly, for the Los Angeles site, NH_3 and CO enhancements are observed during 2020 and 2021 (Figure A3, which can be attributed to the exceptional California fires (Keeley and Syphard, 2021; Safford et al., 2022; Ayars et al., 2023).

For the Izana site, the enhancements observed in 2012 are from the Tenerife Island fire that reached the site in July 2012 (Santamarta Cerezal, 2013). In addition, in September 2021, a volcanic eruption on the island of La Palma (Canary Islands) affected the Izana site (García et al., 2023; Campeny et al., 2023). Studies on NH_3 emissions from volcanic eruptions are limited, but simultaneous enhancements of NH_3 and SO_2 from volcanoes has been reported (Uematsu et al., 2004; Adams et al., 2017), Figure A5 shows SO_2 and NH_3 enhancements during the Tajogaite eruption from 19 September 2021 to 13 December 2021 during which volcanic plume reached the Izana site.

For the analysis in the following sections, the sites are divided into three categories: Arctic (Eureka, Ny Alesund, Thule), Northern Hemisphere (St. Petersburg, Bremen, Garmisch, Zugspitze, Jungfraujoch, Toronto, Boulder, Tsukuba, Los Angeles,

https://doi.org/10.5194/egusphere-2026-3138
Preprint. Discussion started: 15 June 2026

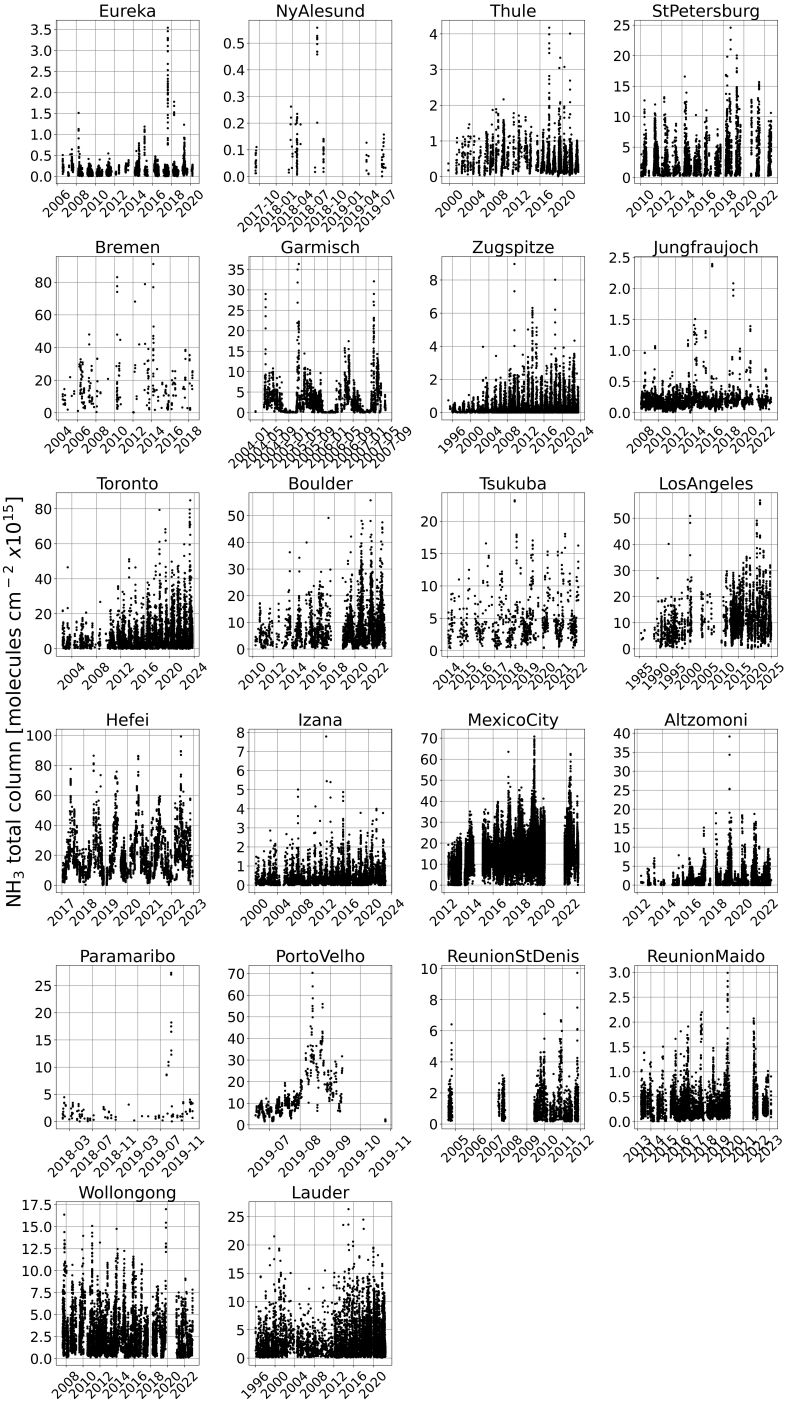

Figure 1. Time series of NH_3 total columns measured at the 22 FTIR sites.

https://doi.org/10.5194/egusphere-2026-3138
Preprint. Discussion started: 15 June 2026

Hefei, Izana, Mexico City, Altzomoni and Paramaribo), and Southern Hemisphere (Porto Velho, Reunion St. Denis, Reunion Maido, Wollongong, and Lauder).

3.2 Seasonal Variability

The seasonal variability in NH_3 total columns corresponding to the monthly means calculated across all years is shown in Figure 2. The seasonal patterns present similarities across most sites, with a few exceptions. In addition, the monthly means are seen to increase for the most recent years for most sites. The monthly mean total columns vary between 0.03 and 42.38×10^{15} molec. cm^{-2} for all sites, with the maximum during spring and summer and the minimum in winter. For the Arctic sites, the variability of NH_3 across the year (between February and October due to the lack of sunlight for FTIR measurements during the Arctic winter) is small. The columns are between 0.06 and 0.70×10^{15} molec. cm^{-2} with the minimum in March and the maximum in August at all three sites, and an average of 0.40×10^{15} molec. cm^{-2}, mainly due to NH_3 being transported from large biomass burning events in northern latitudes, such as the August wildfires in 2017 (Lutsch et al., 2019). The seabirds' nesting season in the Arctic occurs between May and September, and can be a significant N-input source of NH_3 to terrestrial Arctic ecosystems (Wentworth et al., 2016). According to Riddick et al. (2012), the seabird colonies near Thule are larger than those near Eureka, and the difference in the magnitude of the NH_3 columns between these sites is attributed to this source, as shown by Lutsch et al. (2019), mainly due to the presence of seabird colonies on the Greenland coast (Murphy et al., 2025).

For the sites located in the Northern Hemisphere, excluding the Arctic sites, the monthly mean NH_3 total columns vary between 0.03 and 42.38×10^{15} molec. cm^{-2}, with the largest values observed between April and August and the smallest values during December and January. For most sites, NH_3 has a maximum in April and May, then decreases, with another maximum in August in a few cases. However, the maximum monthly mean was found at Hefei in June (42.38×10^{15} molec. cm^{-2}) and the minimum at Zugspitze in December (0.03×10^{15} molec. cm^{-2}). The observed pattern could reflect the influence of the meteorological conditions, mainly related to the NH_3 temperature sensitivity, as warmer temperatures favour the conditions for NH_3 volatilization (Sutton et al., 2013), and the rainfall, which favours wet deposition (Behera et al., 2013). Figure B3 shows the monthly means of surface temperature derived from GCHP.

However, at some sites such as Boulder, a maximum was observed later in the year, probably due to the fertilizer application season and agricultural practices. For Toronto, Mexico City, and Altzomoni, the seasonal patterns were directly compared with those reported in Yamanouchi et al. (2021) and Herrera et al. (2022) as those studies also used these FTIR datasets. For Toronto, the previously reported means were calculated between 2002 and 2018, while this study extends the time series up to 2023; the patterns are very similar with the maximum in May and the minimum in January, however, the columns are larger for April and June in the present study. For Mexico City and Altzomoni, the previously reported time series ended in 2020, while this study extends the time series up to 2022; the patterns are similar with a small increase in the total column means in this study.

For the sites in the Southern Hemisphere, a similar pattern is seen, with more NH_3 during the warmest months, in this case during the last months of the year, with overall monthly mean total columns between 0.21 and 27.82×10^{15} molec. cm^{-2}. The maximum values were found at Porto Velho in August (27.82×10^{15} molec. cm^{-2}) and the minimum at Reunion Maido during March (0.21×10^{15} molec. cm^{-2}). For Porto Velho, it is difficult to isolate a seasonal pattern due to the limited observations,

https://doi.org/10.5194/egusphere-2026-3138
Preprint. Discussion started: 15 June 2026

however, it is clear that August is the month with more NH_3, potentially influenced by Amazonian biomass burning events, in agreement with a study by Whitburn et al. (2015), and specifically for 2019 when an exceptional wildfire event took place in the southern portion of the Amazon during August (Bencherif et al., 2020). Plumes from this fire event could have reached Paramaribo, explaining the enhancements in this site. Overall, the reported seasonal patterns are in agreement with other studies such as Van Damme et al. (2015), which used satellite data. However, this study provides details for the specific sites.

In addition, in Figure 4, the seasonal variability is also shown using a fitted Fourier series of third degree. It can be observed that Eureka, Jungfraujoch, and Reunion Maido have a small seasonal amplitude ($< 0.3 \times 10^{15}$ molec. cm^{-2}). Thule, Zugspitze, Izana, Altzomoni, Wollongong, and Lauder present a moderate seasonal amplitude (between 0.3 and 2×10^{15} molec. cm^{-2}). St. Petersburg, Garmisch, and Tsukuba show a large seasonal amplitude (between 2 and 6×10^{15} molec. cm^{-2}) and Bremen, Toronto, Boulder, Hefei, Los Angeles, and Mexico City have the largest seasonal amplitudes ($> 6 \times 10^{15}$ molec. cm^{-2}). Seasonal variability is markedly smaller at remote and high-altitude sites than at urbanized sites, highlighting the contrast between background atmospheric conditions and regions influenced by anthropogenic and biomass burning emissions.

3.3 Diurnal Variability

One advantage of the FTIR measurements, compared to satellite data, is their frequency, which allows diurnal cycles, during the sunlit part of the day, to be derived by calculating the hourly means as shown in Figure 3 in local hours for the 22 sites. The time series were deseasonalized (Varotsos et al., 2005; Vigouroux et al., 2015) before calculating the diurnal means by subtracting the seasonal component obtained through the evaluation of the fitted Fourier coefficients from Equation 2 at the timestamps of the FTIR time series to estimate the seasonal component at sub-daily resolution. The deseasonalized time series represents anomalies relative to the seasonal mean and can contain both positive and negative values. For Ny Alesund, Paramaribo, Porto Velho, and Reunion St. Denis, the fitting of Fourier series was not possible due to the limited amount of data; therefore, no deseasonalized time series were derived for these sites.

In this case, similar to the monthly means, larger columns are observed for the most recent years for most sites, however, the diurnal variability is very different across the sites, with hourly means between 0.004 and 30.33×10^{15} molec. cm^{-2}. Of the three Arctic sites, Thule showed the most complete diurnal cycle, while very little diurnal fluctuation is observed at these sites, with a mean of 0.47×10^{15} molec. cm^{-2} and a variation of less than 0.5×10^{15} molec. cm^{-2} during the day. This pattern is expected as there are limited sources in the Arctic region that change daily NH_3 concentrations. For the other sites located in the Northern Hemisphere, the diurnal means were between 0.004 and 30.33×10^{15} molec. cm^{-2} with the larger values in the afternoon between around 15h and the minimum in the early morning.

For the Southern Hemisphere, the diurnal means were between 0.10 and 13.68×10^{15} molec. cm^{-2}, smaller values than in the Northern Hemisphere, with no consistent patterns across the sites. However, Lauder presents a pattern similar to Altzomoni, with columns increasing steadily during the day until reaching a peak in the late afternoon. The variability of Altzomoni was explored in Herrera et al. (2022), where this pattern was attributed to NH_3 transported from surrounding urban areas. The high-altitude sites also present very little variability throughout the day, except for Altzomoni.

https://doi.org/10.5194/egusphere-2026-3138
Preprint. Discussion started: 15 June 2026

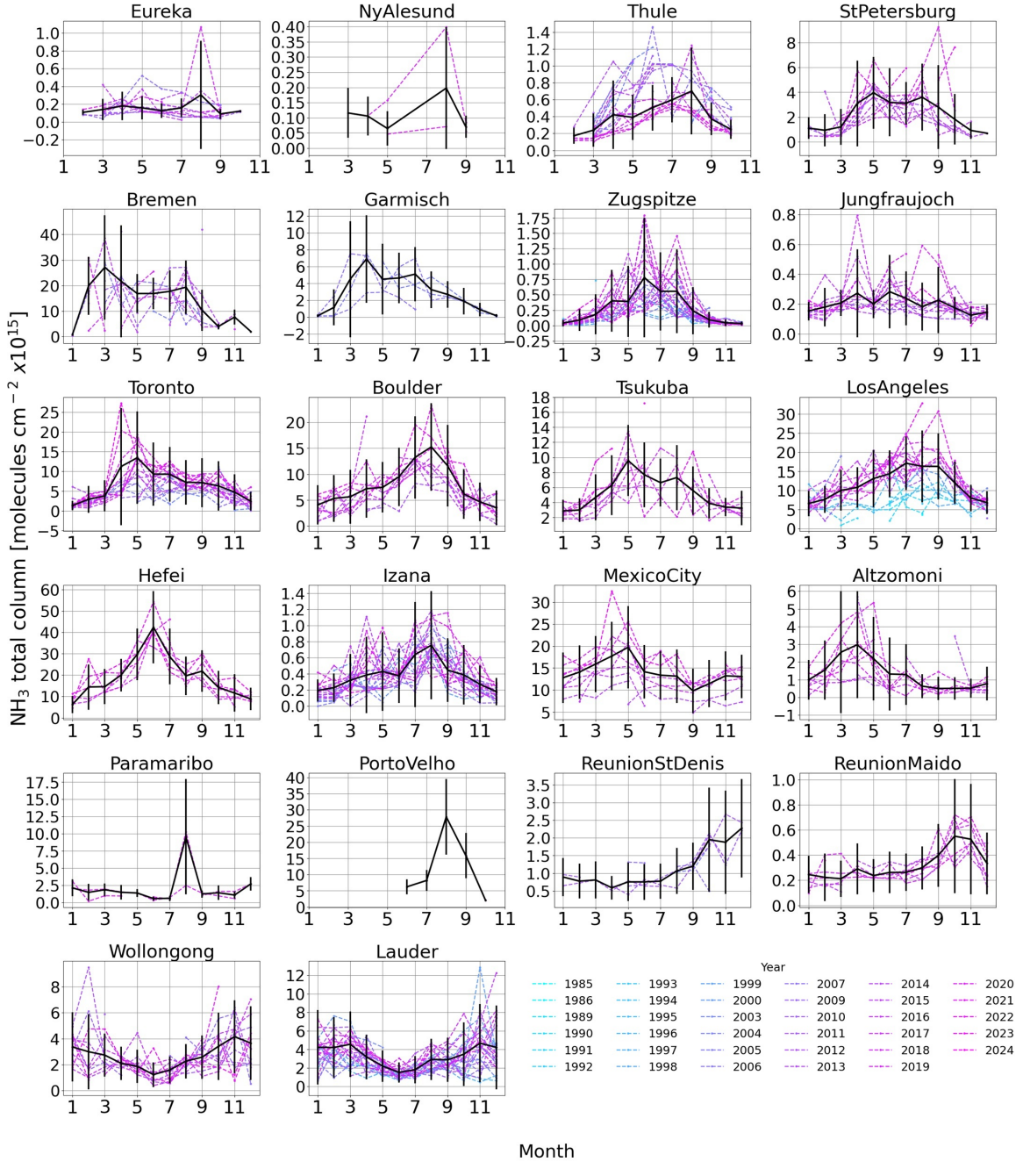

Figure 2. Monthly mean NH_3 total columns for each FTIR site. Different years are shown in different colours, with the most recent years in pink shades and older years in blue shades. The thick black line with error bars is the mean for all years $\pm 1\sigma$.

https://doi.org/10.5194/egusphere-2026-3138
Preprint. Discussion started: 15 June 2026

The reasons for the observed patterns vary depending on each site. Diurnal variations in the NH_3 total columns can be associated with vertical variations of the relative humidity and temperature profiles (Kutzner et al., 2021), as changes in these conditions as well as in the pH can lead to phase changes between NH_3 in the gas and particulate phase (Pye et al., 2020). In addition, transport from the surrounding regions plays a major role in the variability for some sites. Finally, for the sites located in urban areas, traffic emissions during rush hour have an impact on the diurnal variability of NH_3 (Kotnala et al., 2019; Osada et al., 2019; Herrera et al., 2022; Gu et al., 2022; Viatte et al., 2023).

3.4 FTIR Trends

Long-term trends in the daily mean NH_3 total columns are calculated using Eqs. 1 and 2. The FTIR trends, the period used for the trend estimation, and confidence intervals for all sites are summarized in Table 2 and plotted in Figure 4. The mean trend for all sites is 19.43 $(14.18 - 24.68) \times 10^{13}$ molec. cm^{-2} yr^{-1} driven by the large trends at Hefei and Mexico City. Most of the sites present positive and significant trends. Only two sites present negative trends, Thule and Wollongong. Most of the trends are in agreement with trends reported by Van Damme et al. (2021) using ten years of satellite data. The drivers behind these trends vary between sites, and can be due to a change in NH_3 emissions, a change in meteorological conditions, or a change in the lifetime of NH_3 due to changes in NO_x and SO_2 abundances. For the Arctic sites, Thule presents the largest and most significant trend, although it is negative. As mentioned in Section 3.2, seabird colonies are an important source of NH_3 at this site, so changes in the seabird population could impact the trend, such as the reported global decline in seabird population of 69.7% between 1950 and 2010 (Paleczny et al., 2015).

Europe is one of the few regions where actions towards the reduction of NH_3 emissions have been implemented. Zugspitze is located in Germany, where, according to the European Environment Agency (EAP) National Emission Reduction Commitments Directive reporting status 2022 (European Environment Agency, 2023), there have been reductions in NH_3, NO_x, and SO_2 emissions. In addition, Tichý et al. (2023) reported decreasing trends of NH_3 emissions over Europe of -26% over Europe using remote sensing data and inverse modelling analysis. However, the FTIR time series at the five European sites don't show this reduction, suggesting that more efforts focused on reducing NH_3 from the agricultural sector are needed.

Trends in reduced N have been previously reported in North America (Yao and Zhang, 2016; Yamanouchi et al., 2021; Benish et al., 2022; Herrera et al., 2022). In Canada, significant reductions in emissions of SO_x (79%) and NO_x (41%) between 1990 and 2021 have been reported (Government of Canada, 2023). In the US, the Acid Rain Program requires major emissions reductions in SO_2 and NO_x and has delivered annual SO_2 reductions of over 95% and NO_x reductions of over 89% (U.S. Environmental Protection Agency, 2024). These changes could be increasing the atmospheric lifetime of NH_3 over Toronto, Boulder, and Los Angeles, resulting in the positive NH_3 trends. Mexico City has the largest positive and significant trend; this may be due to Mexican policies to regulate NO_x and SO_2 that (similar to Boulder and Toronto) could be affecting the lifetime of NH_3.

For the Southern Hemisphere, the largest trend is from Wollongong, and it is negative. There have been recent efforts in Australia to improve agricultural practices to mitigate emissions of different gases, based on the implementation of technology and a best management practices approach (Panchasara et al., 2021). For NH_3, the focus is on reducing the emissions from

https://doi.org/10.5194/egusphere-2026-3138
Preprint. Discussion started: 15 June 2026

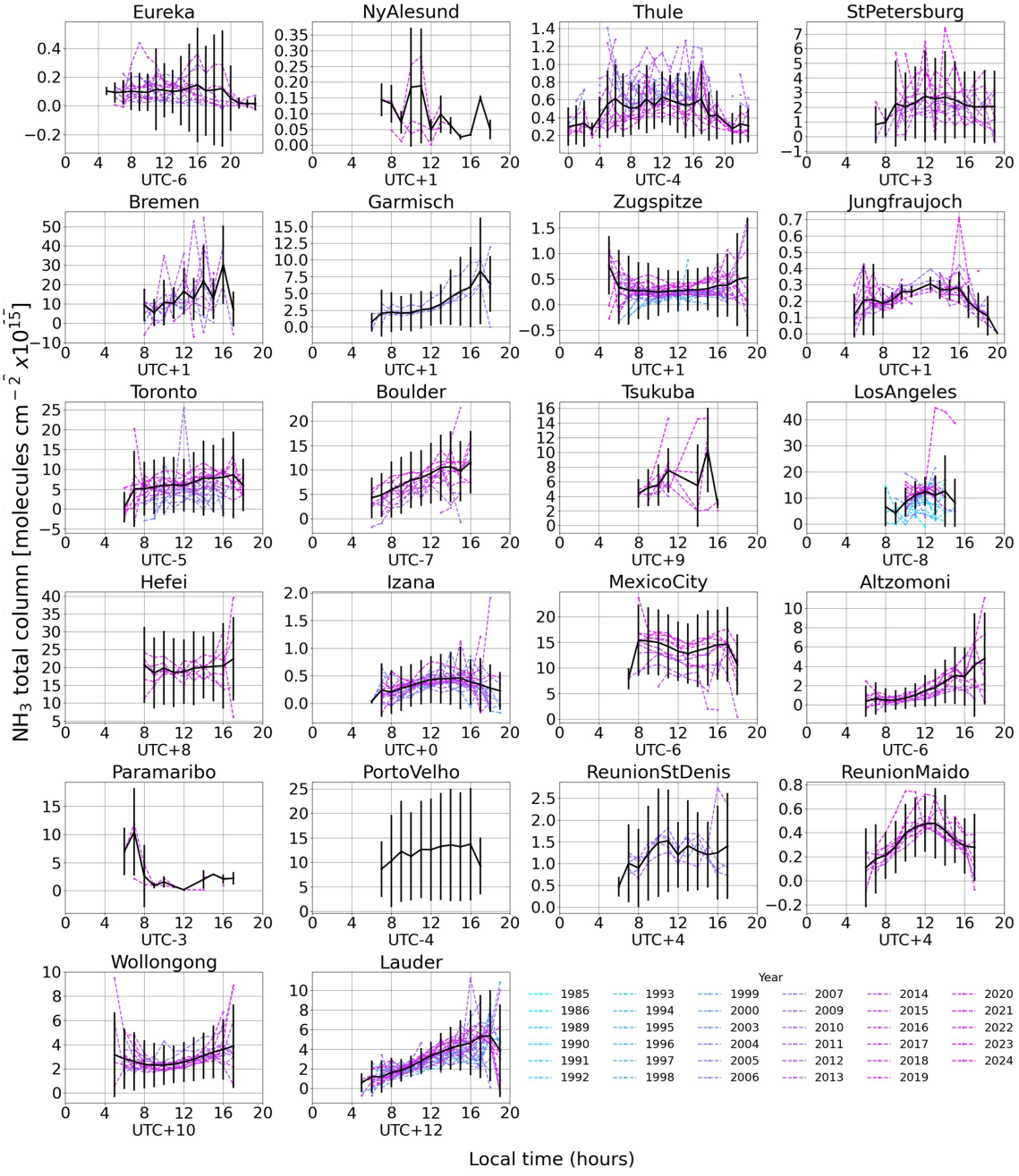

Figure 3. Hourly mean of deseasonalized NH_3 total columns in local time (hours, with offset from UTC for each site indicated on each panel) for each FTIR site. Different years are shown in different colours with the most recent years in pink shades and older years in blue shades. The thick black line with error bars is the mean for all years $\pm 1\sigma$.

https://doi.org/10.5194/egusphere-2026-3138
Preprint. Discussion started: 15 June 2026

Table 2. NH_3 mean total columns $\pm$ 1σ and absolute trends with 95% confidence intervals for the FTIR sites. Bold indicates a significant trend.

Station	Measurement Period	NH_3 Mean Total Column (molec. cm^{-2})$\times 10^{15}$	NH_3 Trend and 95% CI (molec. cm^{-2} yr^{-1})$\times 10^{13}$	%
Eureka	2006 – 2020	0.17 $\pm$ 0.24	**0.58** (0.13 – 1.02)	**3.0** (0.73 – 5.21)
Ny Alesund	2017 – 2019	0.12 $\pm$ 0.12	–	–
Thule	1999 – 2022	0.46 $\pm$ 0.34	**-2.10** (-2.50 – -1.70)	**-7.7** (-9.1 – -6.25)
St. Petersburg	2010 – 2022	3.07 $\pm$ 2.85	**11.70** (3.54 – 19.60)	**4.67** (1.44 – 7.81)
Bremen	2004 – 2018	16.80 $\pm$ 14.70	28.20 (-8.20 – 63.80)	3.55 (-1.03 – 8.02)
Garmisch	2004 – 2007	3.56 $\pm$ 3.97	31.10 (-13.80 – 76.20)	10.64 (-6.39 – 28.04)
Zugspitze	1995 – 2023	0.32 $\pm$ 0.55	**0.84** (0.58 – 1.10)	**2.13** (1.43 – 2.84)
Jungfraujoch	2008 – 2023	0.20 $\pm$ 0.16	**0.38** (0.13 – 0.63)	**1.89** (0.66 – 3.07)
Toronto	2002 – 2023	7.98 $\pm$ 8.53	**28.40** (21.20 – 35.40)	**4.68** (3.53 – 5.82)
Boulder	2010 – 2022	9.00 $\pm$ 7.42	**37.30** (26.30 – 48.30)	**5.93** (4.11 – 7.75)
Tsukuba	2014 – 2022	4.64 $\pm$ 3.45	**19.10** (7.02 – 31.40)	**5.16** (1.82 – 8.46)
Los Angeles	1985 – 2024	11.31 $\pm$ 7.07	**23.4** (19.60 – 27.40)	**4.86** (4.07 – 5.69)
Hefei	2017 – 2022	19.20 $\pm$ 13.50	**73.80** (16.60 – 132)	**4.36** (0.78 – 7.90)
Izana	2000 – 2022	0.42 $\pm$ 0.47	**0.38** (0.03 – 0.74)	**0.88** (0.07 – 1.69)
Mexico City	2012 – 2022	14.50 $\pm$ 6.89	**93.0** (78.8 – 107)	**12.8** (10.86 – 14.79)
Altzomoni	2012 – 2022	1.63 $\pm$ 2.36	**7.08** (2.56 – 11.50)	**10.73** (3.94 – 17.46)
Paramaribo	2018 – 2019	3.02 $\pm$ 4.85	–	–
Porto Velho	2019	11.80 $\pm$ 9.82	–	–
Reunion St. Denis	2004 – 2011	1.21 $\pm$ 1.04	–	–
Reunion Maido	2013 – 2023	0.34 $\pm$ 0.29	0.16 (-0.53 – 0.84)	0.49 (-1.73 – 2.59)
Wollongong	2007 – 2022	2.62 $\pm$ 2.12	**-3.78** (-7.10 – -0.35)	**-0.93** (-1.79 – -0.08)
Lauder	1996 – 2022	3.15 $\pm$ 2.95	**2.37** (0.86 – 3.85)	**1.63** (0.60 – 2.61)
Mean for all sites	–	–	**19.43** (14.18 – 24.68)	**3.82** (3.29 – 4.35)

https://doi.org/10.5194/egusphere-2026-3138
Preprint. Discussion started: 15 June 2026

volatilization by improving the irrigation methods, use of urease inhibitors, and use of ammonium-based fertilizers instead of urea (Pan et al., 2016). Zhang et al. (2022) emphasized the costs and benefits of NH_3 abatement in this region because the mitigation potential of NH_3 emissions from agricultural sources is around 32%. Similarly to Wollongong, several approaches to mitigate NH_3 emissions have been analyzed for New Zealand (Jarvis and Ledgard, 2002; Parfitt et al., 2008; Saggar et al., 2013). Despite this, the trend for Lauder is positive and significant. Around 50% of Australia's and New Zealand's land area is used for agriculture (Pannell and Rogers, 2022). However, there are substantial differences in their agricultural sectors and diversity, with more diversification in Australia and dominance of livestock grazing and dairy production in New Zealand (Pannell and Rogers, 2022). Dairy farms involve several emission sources, such as grazing, fertilizer application, housed animals, and stored and applied excreta (Jarvis and Ledgard, 2002). Implementing strategies to mitigate emissions from several sources is more challenging, and this could be related to Lauder's positive trend. A more detailed discussion of similarities and differences in policy approaches regarding the agricultural situation in New Zealand and Australia is discussed in Pannell and Rogers (2022).

4 Comparison of Simulated NH_3 Total Columns

The FTIR measurements were used to evaluate the simulations of NH_3 by GCHP and TCR-2. Long-term time series of NH_3 total columns were extracted from the previously described GCHP model and TCR-2 product at the grid point closest to the latitude and longitude of each FTIR station. The total columns from GCHP and TCR-2 were smoothed using the FTIR averaging kernels (AVKs) and a priori profiles for each site following the methodology of Rodgers and Connor (2003). The temporal coincidence criterion for matching the simulation and the FTIR observations was 2 h. The time series of NH_3 total columns from FTIR, GCHP and TCR-2 are shown in Figure B2 of the Appendix.

To compare the simulated and FTIR total columns, correlations for the simulation-measurement pairs were performed, in addition to the calculation of simulation minus measurement relative differences (RD) as defined by Equation 3 (Dammers et al., 2016), where $TC_{S,i}$ and $TC_{F,i}$ are the total columns for the simulations and FTIR, respectively. The mean is calculated to obtain the mean relative difference (MRD) for site i between the simulation and the FTIR measurements:

$$MRD = \frac{1}{N}\sum_{i=1}^{N} RD = \frac{1}{N}\sum_{i=1}^{N}\left(\frac{TC_{S,i} - TC_{F,i}}{TC_{F,i}}\right) \times 100. \quad (3)$$

The normalized root mean square error (NRMSE) was calculated with Equation 4, where N is the total number of model-measurement pairs, and σ_F is the standard deviation of the FTIR data, following Kärnä and Baptista (2016) and Flood et al. (2024):

$$NRMSE = \frac{1}{\sigma_F}\sqrt{\sum_{i=1}^{N}(TC_{S,i} - TC_{F,i})^2}. \quad (4)$$

A NRMSE close to 1 indicates a RMSE comparable to σ_F, NRMSE > 1 indicates a RMSE $> \sigma_F$ and poor fit, and NRMSE < 1 indicates a RMSE $< \sigma_F$ and a better agreement of the simulation with respect to the FTIR. Linear regressions were fitted

https://doi.org/10.5194/egusphere-2026-3138
Preprint. Discussion started: 15 June 2026

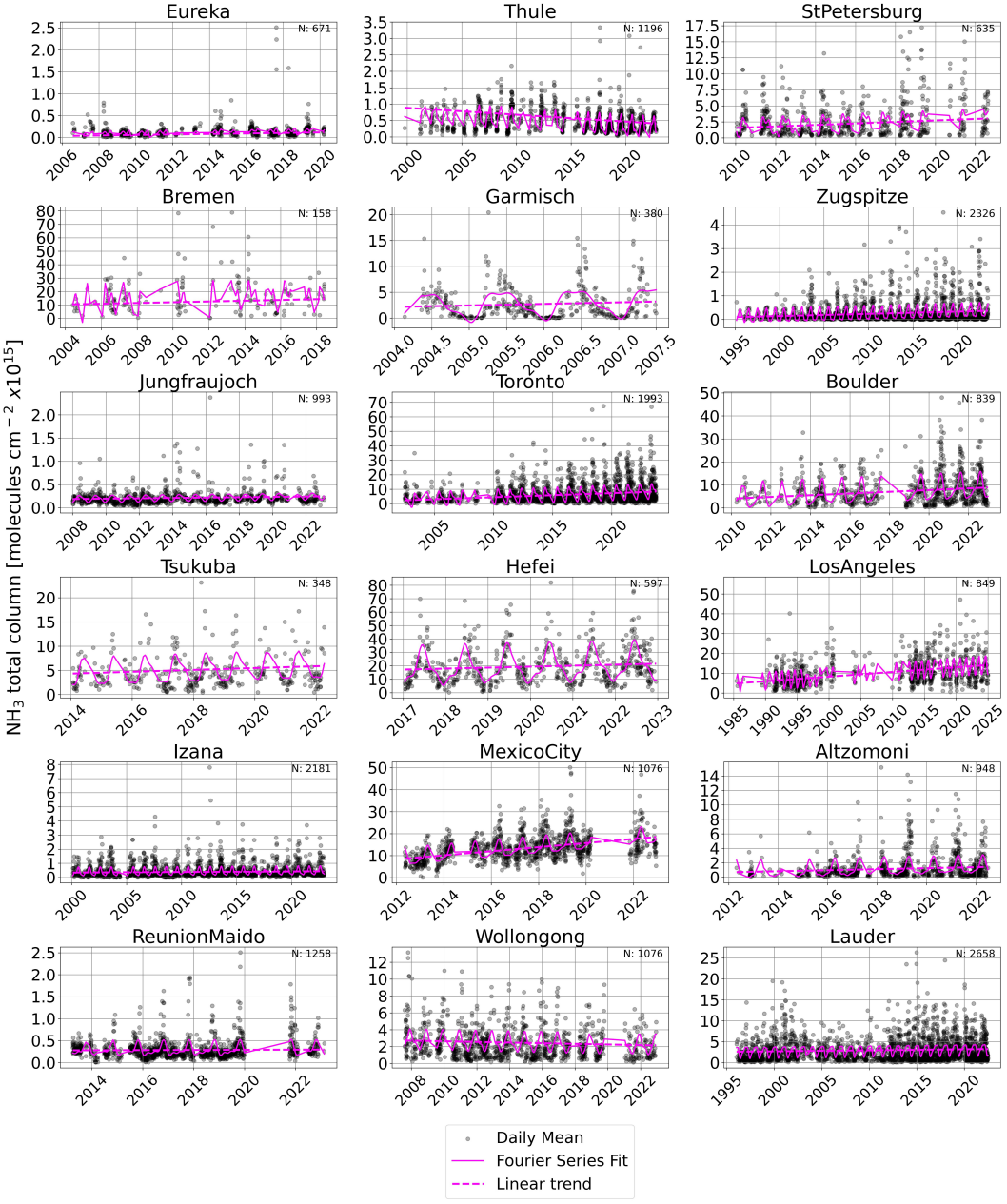

Figure 4. Time series of FTIR daily mean NH_3 total columns with fitted third-order Fourier series (solid blue line) and linear trends (dashed blue line) for the sites with sufficient data density (N) to derive trends.

https://doi.org/10.5194/egusphere-2026-3138
Preprint. Discussion started: 15 June 2026

to the scatter plot data of the GCHP and TCR-2 outputs versus the FTIR measurements, without forcing the intercept to zero. The results are summarized in Table 3, including the correlation coefficient *R*, the fitted slope, the MRD, and the NRMSE. Figure 5 shows the correlations between both datasets and the FTIR data at each station.

Table 3. Results of the NH_3 total column comparisons of GCHP and TCR-2 with the FTIR measurements.

Station	GCHP				TCR-2			
	R	Slope (molec. cm^{-2})×10^{15}	MRD %	NRMSE	*R*	Slope (molec. cm^{-2})×10^{15}	MRD %	NRMSE
Eureka	0.02	0.03	-30.18	1.97	0.81	0.05	-97.23	1.14
Ny Alesund	0.07	0.12	105.93	2.13	0.85	0.06	-73.63	1.19
Thule	0.09	0.47	316.31	6.60	0.12	0.02	-97.63	1.59
St. Petersburg	0.51	0.45	-18.63	0.96	0.39	0.16	-67.73	1.19
Bremen	0.12	0.07	-24.40	1.14	0.23	0.11	-14.45	1.02
Garmisch	0.28	0.50	217.42	2.64	0.18	0.20	111.83	1.66
Zugspitze	0.34	0.55	137.42	1.75	0.36	0.32	-0.32	1.07
Jungfraujoch	0.32	0.34	-19.19	1.23	0.26	0.08	-91.97	1.46
Toronto	0.65	0.39	-44.90	0.88	0.36	0.22	-16.74	0.98
Boulder	0.50	0.34	-18.96	0.92	0.46	0.08	-88.03	1.40
Tsukuba	0.48	1.16	-5.65	2.11	0.45	0.47	-23.64	1.12
Los Angeles	0.55	0.24	-64.47	1.37	0.45	0.26	-42.63	1.20
Hefei	0.40	0.86	-18.78	1.96	0.07	0.15	97.18	2.56
Izana	0.18	0.19	-16.12	0.61	-0.04	0.11	-96.18	0.65
Mexico City	0.38	0.13	-79.02	1.89	0.16	0.03	-88.09	2.13
Altzomoni	0.49	0.11	-73.93	1.04	0.22	0.00	-96.01	1.21
Paramaribo	0.08	0.01	-85.00	1.13	0.09	0.00	-97.06	1.72
Porto Velho	0.85	0.68	-31.02	0.64	NA	NA	NA	NA
Reunion St. Denis	0.22	0.05	-80.41	1.34	-0.02	0.00	-74.63	1.33
Reunion Maido	0.59	0.11	-83.87	1.33	0.13	0.00	-98.86	1.60
Wollongong	0.49	0.37	-11.36	0.91	0.23	0.09	-62.69	1.26
Lauder	0.28	0.12	-56.70	1.15	0.25	0.09	-55.49	1.13
Mean for all sites	0.36	0.27	0.66	1.62	0.28	0.22	-51.14	1.36

The comparisons vary from site to site and differ between GCHP and TCR-2. For GCHP, *R* varies from a minimum of 0.02 at Eureka, to a maximum of 0.85 at Porto Velho. For TCR-2, *R* varies from a minimum of -0.02 at Reunion St. Denis, to a maximum of 0.85 at Ny Alesund. GCHP overestimates NH_3 at two of the three Arctic sites, with poor correlations, large NRMSE, and large columns in the lower range of FTIR, while TCR-2 underestimates NH_3 at all three sites, but with better correlations and NRMSE. For the other Northern Hemisphere sites, the correlation coefficients for GCHP improved,

https://doi.org/10.5194/egusphere-2026-3138
Preprint. Discussion started: 15 June 2026

with larger R = 0.65 for Toronto. GCHP underestimates NH_3 for all sites except Garmisch and Zugspitze, where it significantly overestimates the NH_3 column with large NRMSE values. For TCR-2, the correlations are mostly smaller than those for GCHP, with negative MRDs, a maximum R of 0.46 for Boulder, and a minimum of -0.04 at Izana, while the highest NRMSE are for Hefei and Mexico City. For the Southern Hemisphere, GCHP correlation coefficients are between R = 0.85 and 0.22, with the best correlation for Porto Velho and the smallest value for Reunion St. Denis, with negative MRDs and NRMSE values close to one. For TCR-2, similarly to the Northern Hemisphere sites, the correlations are small, between R = 0.25 for Lauder and R = -0.020 for Reunion St. Denis. TCR-2 continues underestimating NH_3 with negative MRDs and NRMSE > 1.

Using all the available coincidences for all sites, there is an overall correlation coefficient of R = 0.36 and a slope of 0.27 (± 0.002) for GCHP and R = 0.28 and a slope of 0.22 (± 0.003) for TCR-2 as shown in Figure B1 of the Appendix. Figure 5 shows that the GCHP and TCR-2 total columns are larger than the FTIR measurements at the lower range of values, with larger columns from TCR-2 than GCHP. Both model datasets performed similarly at the higher range of values, with lower columns than the FTIR values.

4.1 Seasonal Variability

Figure 6 shows the FTIR, GCHP, and TCR-2 monthly mean NH_3 total columns, including the temporally matched FTIR and models data (solid lines) and the complete time series (dashed lines) between 2003-2021 for GCHP and 2005-2018 for TCR-2. The RD was calculated for each month for each site; then, using the monthly means, the MRD was obtained as reported in Table 4. Overall, no major differences were observed between the dashed and solid lines in Figure 6. Both GCHP and TCR-2 captured similar variability as the FTIRs; however, there are some sites where the differences are more noticeable. Using data for all sites, the analysis suggested a monthly MRD = 0.41% for GCHP and -49.25% for TCR-2. For the Arctic sites, GCHP mainly overestimates and TCR-2 consistently underestimates NH_3 compared to the FTIR observations, while GCHP captures more variability than TCR-2. For the rest of the Northern Hemisphere sites, the best agreements were for Jungfraujoch, Boulder, and Tsukuba for GCHP, and Bremen, Zugspitze, Toronto, and Tsukuba for TCR-2, respectively, but overall, both datasets mainly underestimate NH_3 at all sites. For the Southern Hemisphere, GCHP and TCR-2 presented similar results. For Porto Velho, GCHP and TCR-2 captured the NH_3 maximum between August and September; moreover, GCHP was able to capture the August 2019 enhancement. Both datasets underestimated NH_3 and barely captured the variability for Reunion St. Denis and Reunion Maido. For Wollongong, GCHP is in good agreement with FTIR, while TCR-2 captures the variability but with an underestimation, as in Lauder, where both datasets represented the variability but underestimated the monthly means.

4.2 Diurnal Variability

The NH_3 simulations do not have diurnal variation in anthropogenic emissions; however, in this section, comparisons of the hourly means were performed to assess the ability of GCHP and TCR-2 to capture diurnal variability based on all the other processes involved in the simulations, such as the chemistry, transport, and meteorology variations. For this section, the FTIR and simulated time series of NH_3 total columns were not deseasonalized, as the deseasonalized and regular time series were

https://doi.org/10.5194/egusphere-2026-3138
Preprint. Discussion started: 15 June 2026

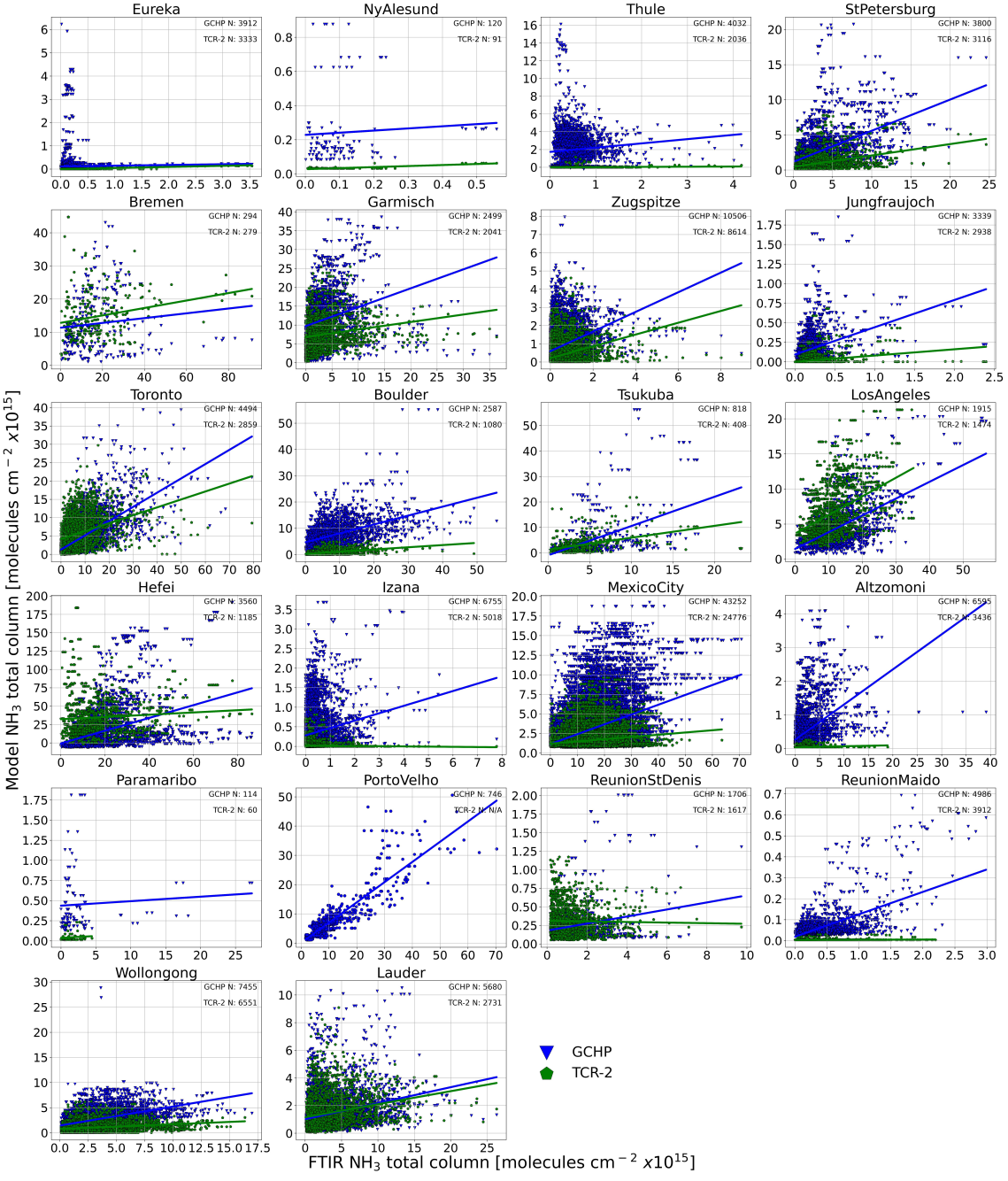

Figure 5. Scatter plots of GCHP and TCR-2 vs. FTIR NH_3 total columns. The lines show the individual regression results for each dataset. Note that for Porto Velho only the correlation between FTIR and GCHP is shown, as there are no TCR-2 data available for this site.

https://doi.org/10.5194/egusphere-2026-3138
Preprint. Discussion started: 15 June 2026

Table 4. MRD for monthly means of GCHP and TCR-2 NH_3 total columns compared to FTIR measurements at each site.

Station	GCHP MRD	TCR-2 MRD
	%	%
Eureka	-41.87	-97.06
Ny Alesund	128.64	-77.99
Thule	265.41	-97.81
St. Petersburg	-23.21	-59.97
Bremen	-21.95	-5.84
Garmisch	233.47	132.21
Zugspitze	140.81	-2.19
Jungfraujoch	-9.88	-90.98
Toronto	-46.41	-18.35
Boulder	-18.12	-88.79
Tsukuba	1.46	-15.92
Los Angeles	-62.78	-42.66
Hefei	-22.92	93.02
Izana	-21.63	-87.18
Mexico City	-80.06	-87.98
Altzomoni	-72.85	-95.62
Paramaribo	-78.99	-96.05
Porto Velho	-28.12	NA
Reunion St. Denis	-80.81	-72.30
Reunion Maido	-84.11	-98.80
Wollongong	-11.69	-66.89
Lauder	-55.28	-57.11
All sites	0.41	-49.25

https://doi.org/10.5194/egusphere-2026-3138
Preprint. Discussion started: 15 June 2026

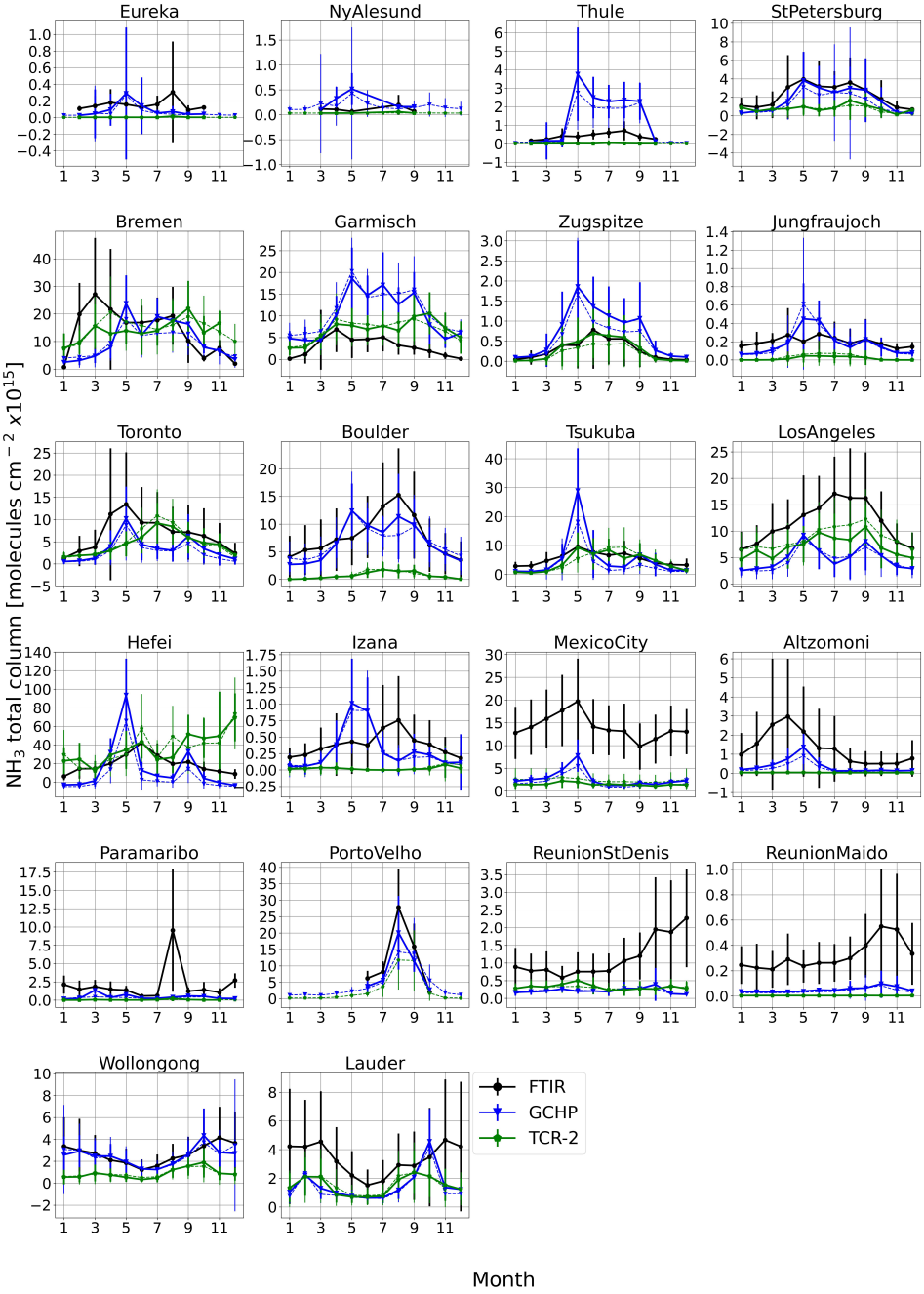

Figure 6. Monthly mean NH_3 total columns FTIR (black), GCHP (blue), and TCR-2 (green). The thick solid lines represent the temporally matched FTIR measurements and GCHP and TCR-2 datasets; the dashed lines represent the complete time series from each dataset. Vertical lines represent the standard deviation ($\pm 1\sigma$).

https://doi.org/10.5194/egusphere-2026-3138
Preprint. Discussion started: 15 June 2026

comparable with a mean $R = 0.92$ for all sites. The hourly means are plotted in Figure 7; the RD was calculated for the matching hours for each site, then the MRD of these hourly means was obtained as shown in Table 5.

There are large differences between the simulated and the measured total columns, as both GCHP and TCR-2 struggled to capture the diurnal variability of NH_3, with an hourly MRD for all sites of 25.47% for GCHP and -47.84% for TCR-2. For the Arctic sites, TCR-2 doesn't capture any diurnal variability, while GCHP seems to capture some variability but with large overestimations, mainly at Ny Alesund and Thule. GCHP performed better at St. Petersburg and Wollongong and TCR-2 at Zugspitze where both datasets effectively reproduced the diurnal cycles, however, in most of the cases, there are large negative biases as observed in Figure 7 and Table 5, except for TCR-2 at Hefei and Garmisch where there is overestimation for the matching time series but better agreement with the full time series. The 24-hour variability from GCHP and TCR-2 could be relevant for some sites, but overall both simulations are unable to capture the diurnal variability of the FTIR instruments.

Table 5. MRD for diurnal means of GCHP and TCR-2 NH_3 total columns compared to FTIR measurements at each site.

Station	GCHP MRD	TCR-2 MRD
	%	%
Eureka	19.91	-96.83
Ny Alesund	234.15	-46.67
Thule	494.09	-97.13
St. Petersburg	9.50	-58.29
Bremen	-35.23	21.35
Garmisch	261.96	109.41
Zugspitze	122.25	-2.38
Jungfraujoch	-36.98	-88.93
Toronto	-40.25	-23.19
Boulder	-16.39	-87.80
Tsukuba	70.75	-35.75
Los Angeles	-42.38	-42.61
Hefei	-22.83	92.72
Izana	-21.35	-96.05
Mexico City	-80.67	-84.95
Altzomoni	-73.51	-96.00
Paramaribo	-39.68	-94.66
Porto Velho	-26.96	NA
Reunion St. Denis	-79.91	-71.91
Reunion Maido	-83.98	-98.71
Wollongong	-9.89	-64.02
Lauder	-42.25	-42.21
All sites	25.47	-47.84

https://doi.org/10.5194/egusphere-2026-3138
Preprint. Discussion started: 15 June 2026

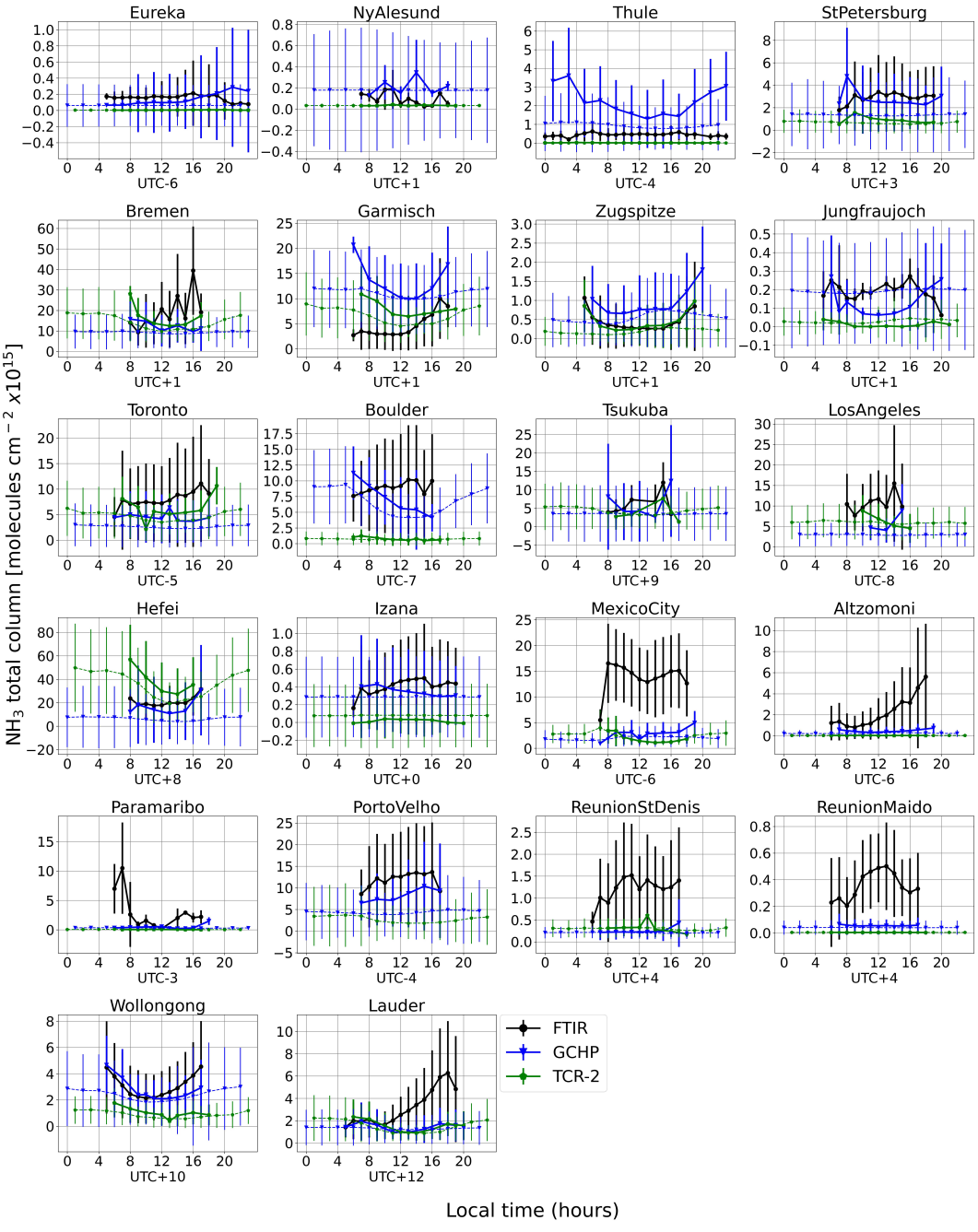

Figure 7. Hourly mean NH_3 total columns of FTIR (black), GCHP (blue), and TCR-2 (green) in local time (hours, with offset from UTC for each site indicated on each panel) for each site. The thick solid lines represent the temporally matched datasets between the FTIR measurements and GCHP and TCR-2 datasets; the dashed lines represent the complete time series from each dataset. Vertical lines represent the standard deviation ($\pm 1\sigma$).

https://doi.org/10.5194/egusphere-2026-3138
Preprint. Discussion started: 15 June 2026

4.3 Sensitivity Tests

Overall, GCHP NH_3 total columns agree better with the FTIR measurements than does TCR-2 for most sites, despite TCR-2 having higher spatial resolution and assimilated observations of relevant tropospheric species. Regardless of the optimization of the emissions and concentrations of various trace gases performed by TCR-2, NH_3 is not among the species that were assimilated. Consequently, the emissions of the TCR-2 NH_3 product in this work are not optimized, and its concentration is only indirectly improved by optimizing species related to the NH_3 chemistry, such as NO_x and SO_2.

One difference between TCR-2 and GCHP is the a priori input emissions inventory used: CEDS for GCHP and HTAP for TCR-2 as described in Section 2.2. To explore the impact of the emissions inventory, we performed sensitivity tests for GCHP by running the model using HTAP emissions for one month (February 2013). In addition, the stand-alone input emissions from HTAP and CEDS were analyzed independently. The MRD difference for the GCHP-HTAP vs. GCHP-CEDS NH_3 total columns and between HTAP and CEDS NH_3 total emissions are presented in Table 6 and were calculated using:

$$MRD = \frac{1}{N}\sum_{i=1}^{N} RD = \frac{1}{N}\sum_{i=1}^{N}\left(\frac{HTAP_{TC/Emissions,i} - CEDS_{TC/Emissions,i}}{CEDS_{TC/Emissions,i}}\right) \times 100. \quad (5)$$

The results show that the GCHP-HTAP NH_3 total columns were, on average 58.90% larger than the respective GCHP-CEDS columns for all sites. The sites with negative HTAP-CEDS MRD in the total columns were Eureka, Tsukuba, and all sites with a latitude south of Izana, while Bremen, Garmisch, Zugstpitze, Jungfraujoch, Toronto, Boulder and Los Angeles presented large positive MRD for the total columns.

The total HTAP NH_3 emissions are 10.85% larger than the total CEDS emissions for all sites, with the biggest differences for Los Angeles, Eureka, Hefei, Boulder and St. Petersburg. Among the emissions, the contribution from anthropogenic and seabird emissions the most different sectors.

This sensitivity test suggests that the larger underestimation in the NH_3 total columns from TCR-2 compared with GCHP is not solely due to the a priori input emissions, since the total columns of GCHP-HTAP were, on average, larger than GCHP-CEDS despite the HTAP emissions being smaller than the CEDS emissions. The systematic negative bias in TCR-2 relative to the FTIR measurements can be related to persistent challenges common to many CTMs. Bian et al. (2017) highlighted that negative biases in NH_3 simulations can result from significant uncertainties in the wet deposition process, where the effective Henry's Law constant for NH_3 varies significantly among different global models, up to six orders of magnitude, depending on what was considered in each model for its calculation (Bian et al., 2017). Additionally, the lack of NH_3 recycling between the atmosphere and soil further contributes to these biases. The implementation of a bi-directional flux scheme has been shown to mitigate these biases, as demonstrated in Zhu et al. (2015) and Cao et al. (2022) for the GEOS-Chem adjoint model. However, this scheme is not included in many CTMs, including the forecast model of TCR-2, limiting its ability to correct for such biases. In the TCR-2 framework, positive model biases in sulfate and nitric acid could also lead to an underestimation of the ratio of gaseous ammonia to particulate ammonium. This issue is partially addressed by optimizing SO_2 and NO_x emissions through data assimilation (Miyazaki et al., 2020a; Sekiya et al., 2023). To further improve the representation of NH_3 in the data

https://doi.org/10.5194/egusphere-2026-3138
Preprint. Discussion started: 15 June 2026

assimilation framework, the most effective approach would be to incorporate improved model schemes while simultaneously assimilating SO_2 and NO_2, along with NH_3 observations.

Table 6. Mean relative differences between GCHP-HTAP and GCHP-CEDS calculated using Equation 5 for NH_3 total columns and NH_3 total emissions for February 2013.

Station	MRD columns	MRD emissions
	%	%
Eureka	-12.01	-99.34
Ny Alesund	9.87	-0.93
Thule	9.00	0.60
St. Petersburg	21.81	-55.79
Bremen	195.69	49.56
Garmisch	210.17	20.45
Zugspitze	210.17	20.45
Jungfraujoch	175.00	27.16
Toronto	121.30	26.21
Boulder	220.52	81.03
Tsukuba	-12.66	-39.37
Los Angeles	213.70	267.64
Hefei	19.87	98.17
Izana	14.31	-67.71
Mexico City	-4.82	-4.11
Altzomoni	-4.82	-4.11
Paramaribo	-14.53	-27.20
Porto Velho	-14.93	-14.77
Reunion St. Denis	-19.20	-7.29
Reunion Maido	-19.20	-7.29
Wollongong	-13.19	-12.05
Lauder	-8.50	-12.64
All sites	58.98	10.85

4.4 Trend Comparison

Long-term trends were derived from the FTIR, GCHP, and TCR-2 datasets using temporally matched daily means as shown in Table 7. The FTIR trends using only the matching data do not indicate major changes compared with the trends in Table 2. The overall GCHP trend is 7.30 (-2.45 – 17.04)$\times 10^{13}$ molec. cm^{-2} yr^{-1}, smaller than the corresponding FTIR value, while the TCR-2 trend is 36.28 (-7.00 – 79.57)$\times 10^{13}$ molec. cm^{-2} yr^{-1}, larger than the FTIR trend, mainly due to the large TCR-2

https://doi.org/10.5194/egusphere-2026-3138
Preprint. Discussion started: 15 June 2026

trend at Hefei. For GCHP, the trend magnitudes are similar to the FTIR trends; however, there are changes in the statistical significance, with the largest differences for the Arctic and Southern Hemisphere sites. For TCR-2, most of the trends were positive but only two were significant. Both GCHP and TCR-2 have differences with the FTIR trends; however, the performance of GCHP is more consistent with the FTIR results than that of TCR-2.

Table 7. Trends in daily mean NH_3 total columns and 95% confidence intervals from GCHP and TCR-2 for daily means temporally matched to the FTIR measurements along with the corresponding FTIR trends. The model profiles were smoothed by the FTIR AVKs prior to calculating total columns. Bold indicates a significant trend.

Station	NH_3 Trends and 95% CI (molec. cm^{-2} yr^{-1})$\times 10^{13}$					
	Time period	FTIR	GCHP	Time	FTIR	TCR-2
Eureka	2006-2020	**0.58** (0.13 – 1.01)	1.12 (-0.31 – 2.58)	2006 -2018	0.48 (-0.10 – 1.07)	0.02 (-0.01 – 0.05)
Thule	2003-2021	**-2.25** (-2.72 – -1.78)	-1.22 (-2.91 – 0.44)	2005-2018	**-2.44** (-3.21 – -1.67)	0.06 (-0.01 – 0.14)
St. Petersburg	2010-2021	**15.1** (5.52 – 24.3)	**9.72** (1.34 – 18.4)	2010-2018	6.83 (-3.27 – 15.7)	-3.34 (-7.34 – 0.60)
Bremen	2004-2018	28.2 (-8.12 – 64.4)	**45.1** (17.2 – 74.5)	2005-2018	18.4 (-19.6 – 58.1)	-6.88 (-30.5 – 16.5)
Garmisch	2004-2007	30.1 (-17.3 – 76.6)	62.2 (-17.9 – 145)	2005-2007	50.7 (-2.67 – 130)	56.4 (-8.59 – 122)
Zugspitze	2003-2021	**0.82** (0.40 – 1.25)	**3.30** (2.64 – 3.98)	2005-2018	**1.32** (0.68 – 1.95)	0.18 (-0.34 – 0.70)
Jungfraujoch	2008-2021	**0.52** (0.21 – 0.82)	**1.61** (1.29 – 1.94)	2008-2018	**0.49** (0.09 – 0.88)	0.09 (-0.05 – 0.23)
Toronto	2003-2021	**31.7** (24.7 – 38.8)	**17.5** (13.1 – 21.8)	2005-2018	**30.6** (19.5 – 41.6)	4.20 (-1.54– 9.86)
Boulder	2010-2021	**45.3** (30.5 – 59.6)	**21.7** (11.8 – 31.6)	2010-2018	**30.6** (5.92 – 55.9)	1.07 (-3.27 – 5.42)
Tsukuba	2014-2021	**16.1** (2.66 – 29.1)	12.6 (-14.5 – 40.6)	2014-2018	-6.09 (-33.3 – 21.9)	**25.1** (3.45 – 45.8)
Los Angeles	2003-2021	**20.9** (3.64 – 3.85)	**16.0** (9.24 – 22.9)	2005-2018	**34.0** (8.07 – 59.4)	9.09 (-6.18 – 24.30)
Hefei	2017-2021	67.8 (-2.02 – 135)	-74.8 (-213 – 64.7)	2017-2018	93.9 (-207 – 395)	564 (-154 – 1310)
Izana	2003-2021	0.32 (-0.17 – 0.82)	**1.69** (1.30 – 2.10)	2005-2018	0.35 (-0.37 – 1.16)	-0.01 (-0.14 – 0.10)
Mexico City	2012-2021	**107** (90.2 – 124)	6.70 (-0.02 – 13.7)	2012-2018	**119** (100 – 137)	1.88 (-1.63 – 5.46)
Altzomoni	2012-2021	**10.7** (5.80 – 15.6)	0.98 (-0.06 – 2.03)	2012-2018	-0.07 (-6.64 – 6.45)	0.05 (-0.02 – 0.12)
Reunion Maido	2013-2021	0.17 (-0.75 – 1.11)	**0.26** (0.08 – 0.45)	2013-2018	**-1.27** (-2.17 – -0.34)	**0.005** (0.001 – 0.01)
Wollongong	2007-2021	-3.34 (-7.17 – 0.52)	**4.17** (1.38 – 7.02)	2007-2018	-4.35 (-9.15 – 0.63)	0.92 (-0.93 – 2.80)
Lauder	2003-2021	2.07 (-0.26 – 4.42)	**2.95** (1.75 – 4.16)	2005-2018	**8.81** (4.96 – 12.6)	0.26 (-1.23 – 1.75)
Mean all	-	**20.66** (15.02 – 26.30)	7.30 (-2.45 – 17.04)	-	**21.18** (2.65 – 39.71)	36.28 (-7.00 – 79.57)

The NH_3 total column trends derived from the full-time series of GCHP and TCR-2 for all sites are shown in Table 8. Overall, most of the GCHP trends are positive and significant, while for TCR-2, there are more negative and fewer significant trends. In addition, GCHP trends are much larger in magnitude than those for TCR-2, and there are differences compared to the trends in Table 7. For GCHP, all the trends for the Arctic sites are small, positive and non-significant; for the Northern Hemisphere all trends were positive and significant, including Hefei; for the Southern Hemisphere only Porto Velho presented a negative trend that is non-significant, while the other sites presented positive trends, including Wollongong. For the Arctic sites, TCR-2 trends are very small and non-significant; for the Northern Hemisphere sites the trends are small and just a few

https://doi.org/10.5194/egusphere-2026-3138
Preprint. Discussion started: 15 June 2026

Table 8. GCHP and TCR-2 trends in NH_3 total columns derived from full time series of each model along with 95% confidence intervals. Bold indicates a significant trend. Model values correspond to the nearest model grid cell to each site (no interpolation applied).

Station	GCHP (2003–2021) NH_3 trends and 95% CI		TCR-2 (2005–2018) NH_3 trends and 95% CI	
	(molec. cm^{-2} yr^{-1})$\times 10^{13}$	%	(molec. cm^{-2} yr^{-1})$\times 10^{13}$	%
Eureka	0.87 (-0.42 – 2.19)	1.99 (-0.97 – 5.01)	0.03 (-0.01 – 0.07)	72.90 (-11.00 – 156.00)
Ny Alesund	**0.90** (0.12 – 1.67)	**3.42** (0.44 – 6.38)	0.05 (-0.01 – 0.11)	29.64 (-3.90 – 62.00)
Thule	0.81 (-0.24 – 1.91)	1.05 (-0.31 – 2.47)	**0.03** (0.00 – 0.07)	**31.11** (2.06 – 58.90)
St. Petersburg	**3.02** (1.69 – 4.27)	**4.09** (2.29 – 5.79)	**-1.12** (-2.13 – -0.14)	**-1.77** (-3.36 – -0.21)
Bremen	**43.80** (39.60 – 48.30)	**6.34** (5.73 – 6.98)	**5.46** (0.98 – 9.99)	**0.59** (0.11 – 1.08)
Garmisch	**19.10** (16.80 – 21.70)	**4.23** (3.72 – 4.79)	**4.10** (0.97 – 7.16)	**0.92** (0.22 – 1.60)
Zugspitze	**19.10** (16.80 – 21.50)	**4.23** (3.70 – 4.76)	**3.58** (0.68 – 6.38)	**0.90** (0.17 – 1.61)
Jungfraujoch	**25.30** (21.80 – 28.60)	**4.74** (4.10 – 5.36)	1.38 (-1.36 – 4.22)	0.37 (-0.36 – 1.12)
Toronto	**12.20** (10.50 – 14.00)	**10.14** (8.73 – 11.60)	2.58 (-0.01 – 5.12)	0.68 (0.00 – 1.35)
Boulder	**12.50** (10.90 – 14.30)	**6.40** (5.54 – 7.29)	0.30 (-0.30 – 0.91)	0.54 (-0.54 – 1.62)
Tsukuba	**8.18** (5.50 – 11.00)	**3.80** (2.55 – 5.10)	**12.80** (9.49 – 16.10)	**5.04** (3.74 – 6.34)
Los Angeles	**7.75** (5.24 – 10.20)	**2.66** (1.80 – 3.50)	-1.55 (-4.85 – 1.81)	-0.26 (-0.80 – 0.30)
Hefei	**41.20** (27.70 – 54.40)	**5.48** (3.69 – 7.24)	**23.70** (9.56 – 37.20)	**1.50** (0.61 – 2.36)
Izana	**3.91** (2.99 – 4.81)	**8.58** (6.57 – 10.60)	-0.19 (-0.51 – 0.12)	-1.59 (-4.38 – 1.05)
Mexico City	**6.20** (4.41 – 7.98)	**3.62** (2.57 – 4.66)	**-1.77** (-2.37 – -1.18)	**2.58** (-3.46 – -1.72)
Altzomoni	**6.16** (4.32 – 7.95)	**3.60** (2.52 – 4.64)	**-1.77** (-2.37 – -1.15)	**2.58** (-3.46 – -1.68)
Paramaribo	**0.64** (0.32 – 0.95)	**1.24** (0.62 – 1.84)	**-0.13** (-0.21 – -0.05)	-2.10 (-3.42 – -0.81)
Porto Velho	**-5.84** (-10.60 – -1.12)	**-1.36** (-2.47 – -0.26)	-5.55 (-11.00 – 0.03)	-1.63 (-3.23 – 0.01)
Reunion St. Denis	**0.11** (0.04 – 0.19)	**0.67** (0.21 – 1.12)	**1.09** (0.94 – 1.24)	**6.51** (5.61 – 7.43)
Reunion Maido	**0.11** (0.04 – 0.18)	**0.65** (0.21 – 1.09)	**1.09** (0.94 – 1.24)	**6.51** (5.61 – 7.44)
Wollongong	**2.69** (0.29 – 5.17)	**1.60** (0.17 – 3.08)	**-1.65** (-2.46 – -0.85)	**-1.95** (-2.90 – -1.01)
Lauder	**4.42** (3.31 – 5.54)	**3.36** (2.52 – 4.22)	-0.02 (-0.74 – 0.68)	-0.02 (-0.59 – 0.54)
Mean for all sites	**10.11** (9.31 – 10.91)	**3.66** (3.35 – 3.97)	**1.93** (1.11 – 2.75)	**6.49** (2.00 – 10.98)

https://doi.org/10.5194/egusphere-2026-3138
Preprint. Discussion started: 15 June 2026

of them are significant, including the negative trend for Mexico City; finally for the Southern Hemisphere, the trend for Porto Velho is also negative but non-significant, while the trend for Wollongong is negative, significant and similar to the FTIR trend.

The NH_3 partitioning at each site was derived using GCHP total columns of NH_3 and NH_4^+ to calculate the NH_3/NH_4^+ ratio and explore which was the predominant species in the chemical equilibrium. In addition, correlations of NH_3 total columns with total columns of SO_2 and NO_x, and surface temperature were calculated. These results are shown in Table 9. The NH_3/NH_4^+ ratio is less than one for all sites except Porto Velho and Lauder, meaning that NH_3 prevails in the particulate phase. This suggests that the previously described model trends might be underestimated, as they were calculated for NH_3 in the gas phase. Most of the correlations with SO_2 and NO_x are very small, with a few exceptions. For Porto Velho, the NH_3/NH_4^+ ratio is 2.93 with R = 0.91 for SO_2 and R = 0.77 for NO_x. This suggests that for Porto Velho, the NH_3 trends are due to changes in the emission sources rather than a reduction in the emissions of SO_2 and NO_x. The correlation coefficients between surface temperature and NH_3 total columns were > 0.5 only for Bremen, Garmisch, Zugspitze, and Jungfraujoch, suggesting that for these sites, temperature changes could have a greater impact on NH_3 concentrations than for other sites.

5 Conclusions

Using NH_3 total columns from ground-based FTIR spectrometers at 22 globally distributed sites and from a global CTM (GCHP) and a reanalysis product (TCR-2), this work examined the variability and trends of atmospheric NH_3. The FTIR time series revealed that NH_3 is present even in the most remote areas, and it can show significant enhancements, mainly due to biomass burning events. The seasonal patterns were similar across most sites, with total columns ranging between 2.66 and 6.92×10^{15} molec. cm^{-2}, and are in agreement with previous studies mainly using satellite data. The patterns are influenced by meteorological conditions such as temperature and rain, seasons of fertilizer application, and fire season. Overall, both NH_3 simulations captured the seasonality of the FTIR measurements with some differences, mainly underestimations for the Northern and Southern Hemisphere sites and GCHP overestimations in the Arctic.

The diurnal variability of NH_3 total columns was shown for the first time for most of the FTIR sites, with total column variations between 0.20 and 6.74×10^{15} molec. cm^{-2} and large differences between sites. In general, the diurnal patterns differ significantly and depend on the characteristics of each site, as well as the influence of local sources such as vehicular emissions and NH_3 transported from surrounding areas in the late afternoon. Both models struggled to capture the diurnal variability of the measurements, mainly due to the lack of diurnal variation in the anthropogenic emissions used in the NH_3 simulations.

Most NH_3 FTIR trends are positive and significant, ranging from 0.38 to 93×10^{13} molec. cm^{-2} yr^{-1} for all sites. The largest trends were for Mexico City, Boulder, and Toronto. The equivalent trends calculated using GCHP and the TCR-2 product were, in general, smaller for both GCHP and TCR-2. The trends using the full time series for GCHP are 10.11 (9.31 – 10.91)$\times 10^{13}$ molec. cm^{-2} yr^{-1} between 2003 and 2021 and 1.93 (1.11 – 2.75)$\times 10^{13}$ molec. cm^{-2} yr^{-1} for TCR-2 between 2005 and 2018. The drivers behind these trends depend on each location, and they involve a combination of changes in the

https://doi.org/10.5194/egusphere-2026-3138
Preprint. Discussion started: 15 June 2026

Table 9. GCHP NH_3/NH_4^+ total column ratio and correlation coefficients for NH_3 total columns vs. SO_2 and NO_x total columns and surface temperature between 2003 and 2021. Model values correspond to the nearest grid cell to each site. Surface temperature was vertically interpolated to station pressure levels to account for unresolved topography.

	Ratio	Correlation coefficient *R* for NH_3 with		
Station	NH_3/NH_4^+	SO_2	NO_x	Surface Temperature
Eureka	0.08	-0.03	0.13	0.07
Ny Alesund	0.08	0.00	0.07	-0.02
Thule	0.20	-0.17	0.48	0.38
St. Petersburg	0.14	-0.06	0.10	0.33
Bremen	0.57	0.02	-0.18	0.64
Garmisch	0.56	-0.15	-0.02	0.52
Zugspitze	0.56	-0.15	-0.02	0.59
Jungfraujoch	0.50	-0.13	-0.19	0.51
Toronto	0.22	-0.15	-0.04	0.40
Boulder	0.52	-0.03	0.39	0.49
Tsukuba	0.16	0.00	-0.06	0.12
Los Angeles	0.59	0.03	0.22	0.17
Hefei	0.23	-0.25	-0.25	0.25
Izana	0.19	0.09	0.30	0.19
Mexico City	0.24	0.40	0.09	0.47
Altzomoni	0.24	0.40	0.09	0.22
Paramaribo	0.92	0.01	-0.07	0.00
Porto Velho	2.93	0.91	0.77	0.41
Reunion St. Denis	0.21	-0.01	-0.14	-0.10
Reunion Maido	0.21	-0.01	-0.14	-0.06
Wollongong	0.55	0.37	0.63	0.26
Lauder	1.20	-0.10	0.17	0.16

https://doi.org/10.5194/egusphere-2026-3138
Preprint. Discussion started: 15 June 2026

NH_3, NO_x, and SO_2 emissions and changes in the meteorology. According to GCHP, NH_3 prevails in the particulate form NH_4^+ at most sites, suggesting that the model trends presented in this work might be underestimated.

Overall, GCHP exhibited a generally better agreement with the FTIR observations than TCR-2, with the largest differences at the Arctic sites and Mexico City. Sensitivity tests regarding the a priori emissions were performed, finding that the differences in the emissions inventories used in GCHP and TCR-2 are not driving the larger underestimation observed in the TCR-2 product. The persistent negative bias in TCR-2 can be related to the lack of a bi-directional exchange flux scheme in its framework and to persistent positive model biases in sulfate and nitric acid. Further sensitivity tests and direct assimilation of NH_3 from satellite observations are recommended to improve the TCR-2 NH_3 product.

NH_3 is a short-lived and highly variable atmospheric trace gas present in urban and remote areas, with consequences for the Earth's radiative forcing balance, ecosystems, and human health, including its role as $PM_{2.5}$ precursor. Atmospheric NH_3 concentrations have been rising since the early 1900s with the introduction of synthetic fertilizers and they continue to increase globally. The lack of global regulation regarding NH_3 emissions, changes in meteorology, and emissions of other species such as NO_x and SO_2 are some of the factors contributing to this. It is important to continue and expand the monitoring of NH_3 using ground-based and satellite instruments to extend the time series of this gas, analyze trends, and reduce uncertainties in the emissions and simulations. Such measurements could help inform the development of global regulations and policies that are needed to reduce the atmospheric concentration of NH_3 and its effects.

Appendix A: NH_3 Enhancements

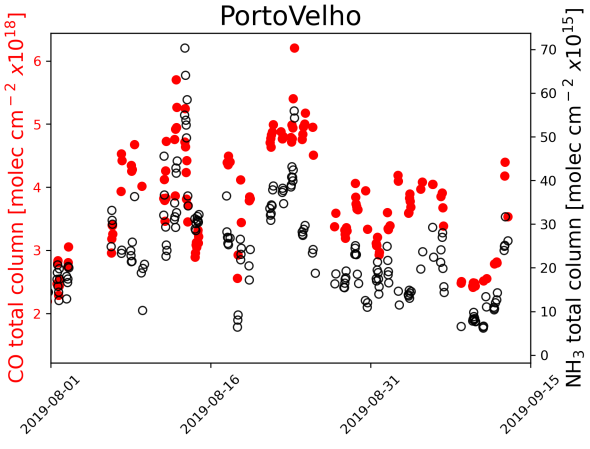

Figure A1. Comparison of NH_3 and CO total columns measured at Porto Velho between July and September 2019. Simultaneous enhancements can be observed, attributed to biomass burning events.

https://doi.org/10.5194/egusphere-2026-3138
Preprint. Discussion started: 15 June 2026

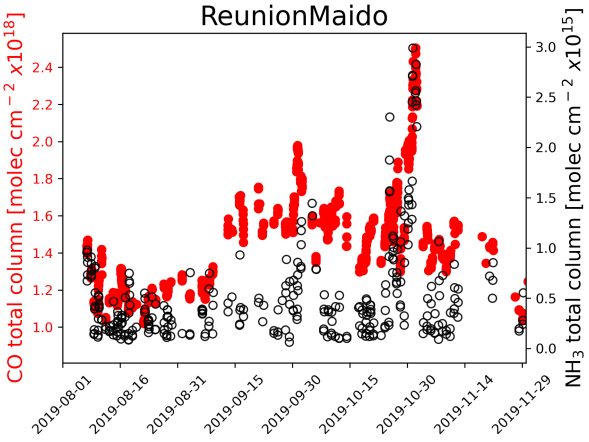

Figure A2. Comparison of NH_3 and CO total columns measured at Reunion Maido between August and November 2019. Simultaneous enhancements can be observed, attributed to biomass burning events.

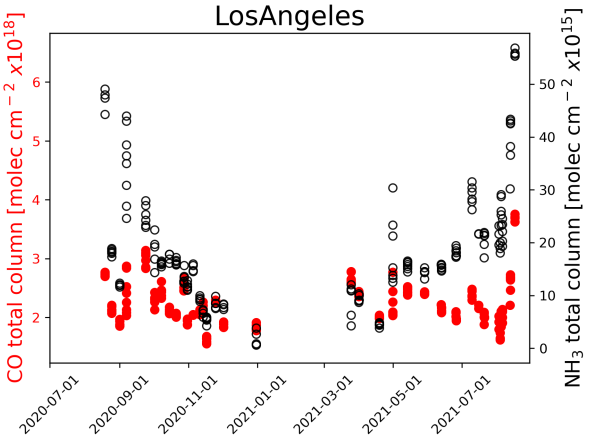

Figure A3. Comparison of NH_3 and CO total columns measured at Los Angeles between July 2020 and August 2021. Simultaneous enhancements can be observed, attributed to wildfires.

https://doi.org/10.5194/egusphere-2026-3138
Preprint. Discussion started: 15 June 2026

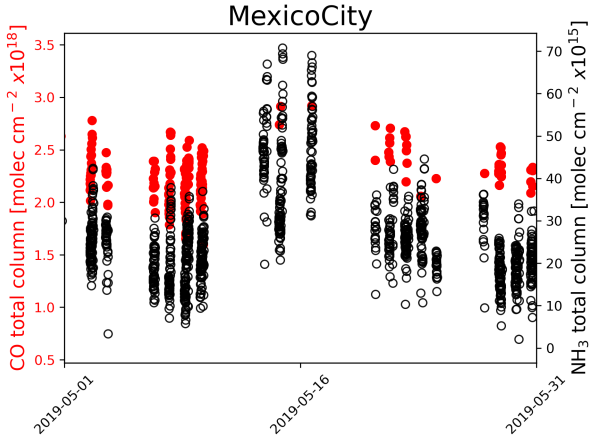

Figure A4. Comparison of NH_3 and CO total columns measured at Mexico City during May 2019. Simultaneous enhancements can be observed, attributed to biomass burning events.

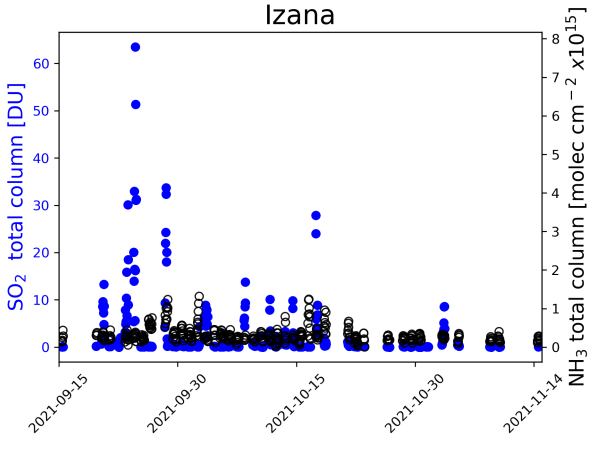

Figure A5. Comparison of NH_3 and SO_2 total columns measured at Izana between September and November 2021 during the Tarjogaite volcanic eruption that reached the Izana site. Simultaneous enhancements can be observed.

https://doi.org/10.5194/egusphere-2026-3138
Preprint. Discussion started: 15 June 2026

Appendix B: Model Comparisons

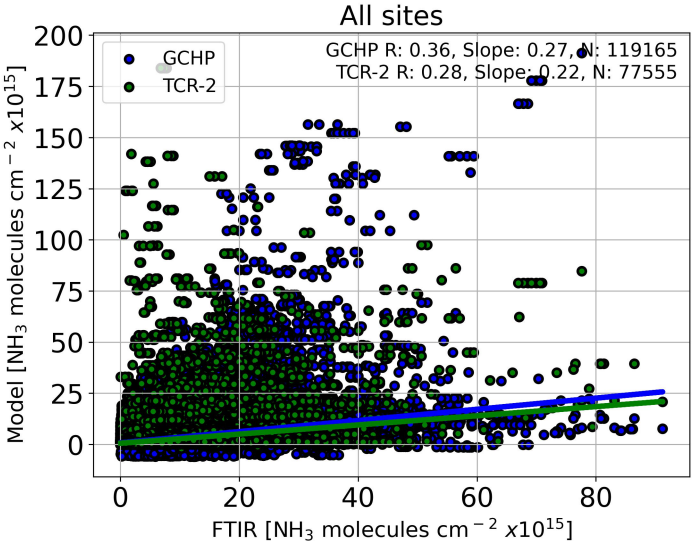

Figure B1. Scatter plot of GCHP and TCR-2 vs. FTIR temporally matched NH_3 total columns. The lines show the regression results for each model.

Data availability. The time series of FTIR NH_3 total columns are available on the Borealis repository at https://doi.org/10.5683/SP3/9UV6KA (Herrera Gutierrez et al., 2025). The TCR-2 products are available via https://tes.jpl.nasa.gov/tes/chemical-reanalysis/ (Miyazaki et al., 2019). The GEOS-Chem High Performance model version 14.1.1 used in this work is freely available to the public via https://doi.org/10.5281/zenodo.7600586 (GEOS-Chem, 2023).

Author contributions. BH, DBAJ, and KS developed the concept of the study. BH wrote the manuscript. KS reviewed all versions of the manuscript. BH, ED, MDM, OG, MG, JWH, NJ, EM, MK, IM, IO, MP, AP, DS, HS, WS, RS, GCT, CV, WW, and KS facilitated the FTIR retrievals. KM contributed to the TCR-2 product. TW, DBAJ, and BH contributed to the GCHP product. All co-authors provided critical review and comments throughout the different versions of the manuscript.

Competing interests. The authors declare that they have no conflict of interest.

Disclaimer. Language editing was assisted using Grammarly. The authors retain full responsibility for the manuscript content.

https://doi.org/10.5194/egusphere-2026-3138
Preprint. Discussion started: 15 June 2026

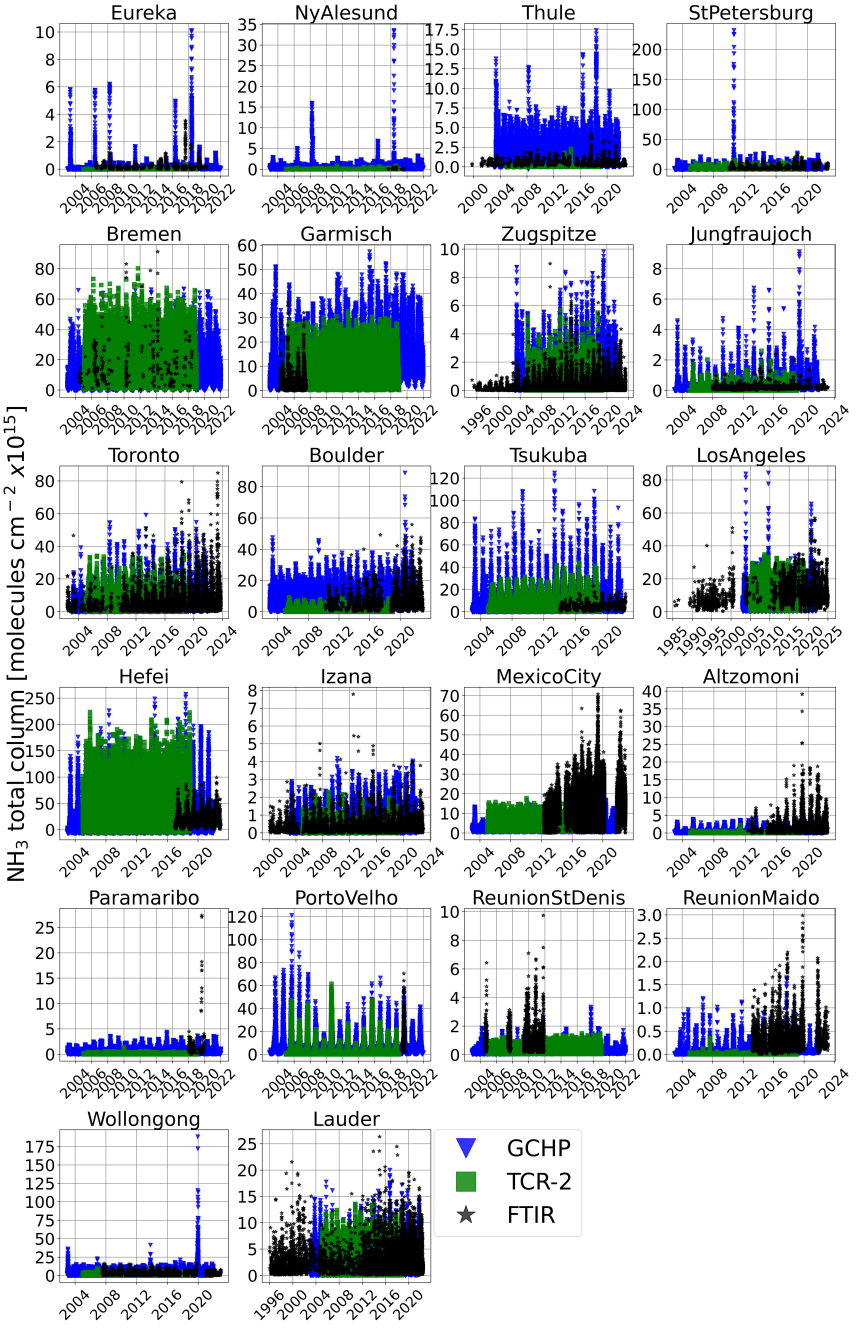

Figure B2. Comparison of the time series of NH_3 total columns from FTIR measurements (black) versus GCHP (blue) and TCR-2 (green) at the 22 FTIR sites.

https://doi.org/10.5194/egusphere-2026-3138
Preprint. Discussion started: 15 June 2026

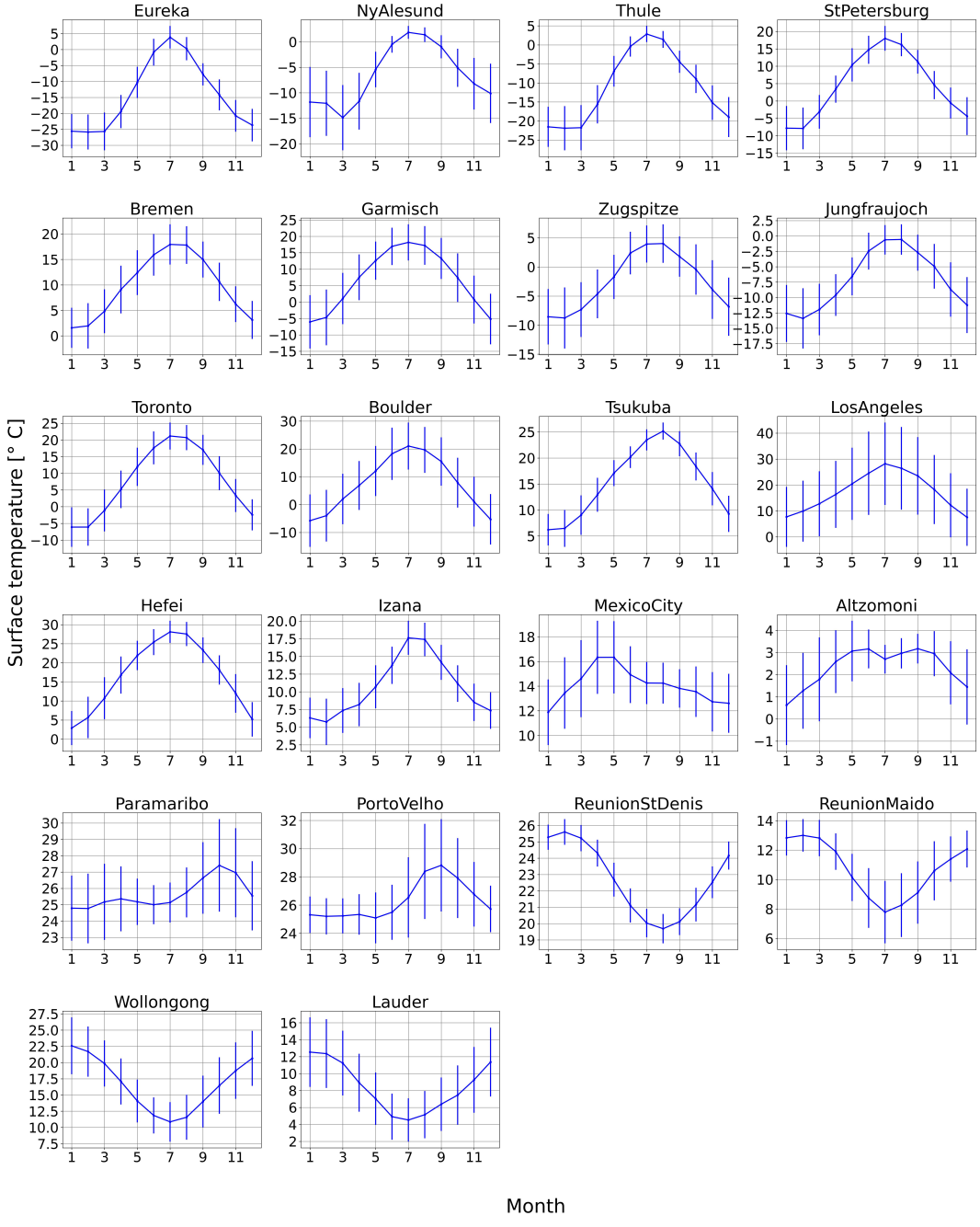

Figure B3. Monthly mean GCHP surface temperature at each FTIR site between 2003 and 2021. Vertical lines represent the standard deviation ($\pm 1\sigma$).

https://doi.org/10.5194/egusphere-2026-3138
Preprint. Discussion started: 15 June 2026

Special issue statement. This article is intended to be part of the "Achievements and perspectives of the Network for the Detection of Atmospheric Composition Change (NDACC) after 35 years of operation (ACP/AMT inter-journal SI)".

Acknowledgements. This research has been supported by the Consejo Nacional de Ciencia y Tecnología (CONACYT, now SECIHTI) (PhD grant no. 665043). Measurements at the Mexico City and Altzomoni sites were supported by the DGAPA-PAPIIT Grants No. IG101225 and IN106024. The Eureka measurements were made at the Polar Environment Atmospheric Research Laboratory (PEARL) by the Canadian Network for the Detection of Atmospheric Change (CANDAC), and the Toronto measurements were made at the University of Toronto Atmospheric Observatory (TAO); both are primarily supported by the Natural Sciences and Engineering Research Council of Canada, the Canadian Space Agency and Environment and Climate Change Canada.

The Tsukuba FTIR operation is supported in part by the GOSAT Series project. The measurements at the University of Bremen are supported by the Senate of Bremen. The measurements at Ny Alesund are supported by the AWI Germany. We thank the personnel at Bremen and Ny Alesund for support in obtaining the measurements. The ULiège contribution to this work was primarily supported by the Fonds de la Recherche Scientifique (F.R.S. – FNRS, Brussels, Belgium) and the GAW-CH program of MeteoSwiss (Zürich, CH). EM is a research director with F.R.S. – FNRS. The ULiège team thanks the International Foundation High Altitude Research Stations Jungfraujoch and Gornergrat (HFSJG, Bern, CH) for supporting the facilities needed to perform the Fourier Transform InfraRed observations at Jungfraujoch. Measurements at Lauder are funded by Earth Sciences New Zealand through New Zealand's Ministry of Business, Innovation and Employment Strategic Science Investment Fund.

The authors acknowledge Saint-Petersburg State University for a research project 132392751 ($GZ_M DF_2026$). We acknowledge the use of data products from the National Aeronautics and Space Administration (NASA) Aura and Terra and Aqua satellite missions. We also acknowledge the support of the NASA Atmospheric Composition: Aura Science Team Program (19-AURAST19-0044), Earth Science U.S. Participating Investigator program (22-EUSPI22-0005), ACMAP (22-ACMAP22-0013), and the NASA TROPESS project. Part of this work was conducted at the Jet Propulsion Laboratory, California Institute of Technology, under contract with NASA. We acknowledge the use of the GFASv1.2 emissions inventory, which contains modified Copernicus Atmosphere Monitoring Service information.

https://doi.org/10.5194/egusphere-2026-3138
Preprint. Discussion started: 15 June 2026

References

Adams, P. M., Lynch, D. K., Buckland, K. N., Johnson, P. D., and Tratt, D. M.: Sulfate mineralogy of fumaroles in the Salton Sea Geothermal Field, Imperial County, California, Journal of Volcanology and Geothermal Research, 347, 15–43, https://doi.org/10.1016/j.jvolgeores.2017.08.010, 2017.

Ayars, J., Kramer, H. A., and Jones, G. M.: The 2020 to 2021 California megafires and their impacts on wildlife habitat, Proceedings of the National Academy of Sciences, 120, e2312909 120, https://doi.org/10.1073/pnas.2312909120, 2023.

Bader, W., Bovy, B., Conway, S., Strong, K., Smale, D., Turner, A. J., Blumenstock, T., Boone, C., Collaud Coen, M., Coulon, A., Garcia, O., Griffith, D. W. T., Hase, F., Hausmann, P., Jones, N., Krummel, P., Murata, I., Morino, I., Nakajima, H., O'Doherty, S., Paton-Walsh, C., Robinson, J., Sandrin, R., Schneider, M., Servais, C., Sussmann, R., and Mahieu, E.: The recent increase of atmospheric methane from 10 years of ground-based NDACC FTIR observations since 2005, Atmospheric Chemistry and Physics, 17, 2255–2277, https://doi.org/10.5194/acp-17-2255-2017, 2017.

Battye, W., Aneja, V. P., and Schlesinger, W. H.: Is nitrogen the next carbon?, Earth's Future, 5, 894–904, https://doi.org/10.1002/2017EF000592, 2017.

Behera, S. N., Sharma, M., Aneja, V. P., and Balasubramanian, R.: Ammonia in the atmosphere: a review on emission sources, atmospheric chemistry and deposition on terrestrial bodies, Environmental Science and Pollution Research, 20, 8092–8131, https://doi.org/10.1007/s11356-013-2051-9, 2013.

Bencherif, H., Bègue, N., Kirsch Pinheiro, D., du Preez, D. J., Cadet, J.-M., da Silva Lopes, F. J., Shikwambana, L., Landulfo, E., Vescovini, T., Labuschagne, C., Silva, J. J., Anabor, V., Coheur, P.-F., Mbatha, N., Hadji-Lazaro, J., Sivakumar, V., and Clerbaux, C.: Investigating the Long-Range Transport of Aerosol Plumes Following the Amazon Fires (August 2019): A Multi-Instrumental Approach from Ground-Based and Satellite Observations, Remote Sensing, 12, https://doi.org/10.3390/rs12223846, 2020.

Benish, S. E., Bash, J. O., Foley, K. M., Appel, K. W., Hogrefe, C., Gilliam, R., and Pouliot, G.: Long-term regional trends of nitrogen and sulfur deposition in the United States from 2002 to 2017, Atmospheric Chemistry and Physics, 22, 12 749–12 767, https://doi.org/10.5194/acp-22-12749-2022, 2022.

Bian, H., Chin, M., Hauglustaine, D. A., Schulz, M., Myhre, G., Bauer, S. E., Lund, M. T., Karydis, V. A., Kucsera, T. L., Pan, X., Pozzer, A., Skeie, R. B., Steenrod, S. D., Sudo, K., Tsigaridis, K., Tsimpidi, A. P., and Tsyro, S. G.: Investigation of global particulate nitrate from the AeroCom phase III experiment, Atmospheric Chemistry and Physics, 17, 12 911–12 940, https://doi.org/10.5194/acp-17-12911-2017, 2017.

Bindle, L., Martin, R. V., Cooper, M. J., Lundgren, E. W., Eastham, S. D., Auer, B. M., Clune, T. L., Weng, H., Lin, J., Murray, L. T., Meng, J., Keller, C. A., Putman, W. M., Pawson, S., and Jacob, D. J.: Grid-stretching capability for the GEOS-Chem 13.0.0 atmospheric chemistry model, Geoscientific Model Development, 14, 5977–5997, https://doi.org/10.5194/gmd-14-5977-2021, 2021.

Callewaert, S., Brioude, J., Langerock, B., Duflot, V., Fonteyn, D., Müller, J.-F., Metzger, J.-M., Hermans, C., Kumps, N., Ramonet, M., Lopez, M., Mahieu, E., and De Mazière, M.: Analysis of CO_2, CH_4, and CO surface and column concentrations observed at Réunion Island by assessing WRF-Chem simulations, Atmospheric Chemistry and Physics, 22, 7763–7792, https://doi.org/10.5194/acp-22-7763-2022, 2022.

Campeny, M., Menéndez, I., Ibáñez-Insa, J., Rivera-Martínez, J., Yepes, J., Álvarez Pousa, S., Méndez-Ramos, J., and Mangas, J.: The ephemeral fumarolic mineralization of the 2021 Tajogaite volcanic eruption (La Palma, Canary Islands, Spain), Scientific Reports, 13, 6336, https://doi.org/10.1038/s41598-023-33387-6, 2023.

https://doi.org/10.5194/egusphere-2026-3138
Preprint. Discussion started: 15 June 2026

Cao, H., Henze, D. K., Zhu, L., Shephard, M. W., Cady-Pereira, K., Dammers, E., Sitwell, M., Heath, N., Lonsdale, C., Bash, J. O., Miyazaki, K., Flechard, C., Fauvel, Y., Kruit, R. W., Feigenspan, S., Brümmer, C., Schrader, F., Twigg, M. M., Leeson, S., Tang, Y. S., Stephens, A. C. M., Braban, C., Vincent, K., Meier, M., Seitler, E., Geels, C., Ellermann, T., Sanocka, A., and Capps, S. L.: 4D-Var Inversion of European NH_3 Emissions Using CrIS NH_3 Measurements and GEOS-Chem Adjoint With Bi-Directional and Uni-Directional Flux Schemes, Journal of Geophysical Research: Atmospheres, 127, e2021JD035 687, https://doi.org/https://doi.org/10.1029/2021JD035687, 2022.

Chen, J., Cheng, M., Krol, M., De Vries, W., Zhu, Q., Liu, X., Zhang, F., and Xu, W.: Trends in anthropogenic ammonia emissions in China since 1980: A review of approaches and estimations, Frontiers in Environmental Science, 11, 1133 753, https://doi.org/10.3389/fenvs.2023.1133753, 2023.

Dammers, E., Vigouroux, C., Palm, M., Mahieu, E., Warneke, T., Smale, D., Langerock, B., Franco, B., Van Damme, M., Schaap, M., Notholt, J., and Erisman, J. W.: Retrieval of ammonia from ground-based FTIR solar spectra, Atmospheric Chemistry and Physics, 15, 12 789–12 803, https://doi.org/10.5194/acp-15-12789-2015, 2015.

Dammers, E., Palm, M., Van Damme, M., Vigouroux, C., Smale, D., Conway, S., Toon, G. C., Jones, N., Nussbaumer, E., Warneke, T., Petri, C., Clarisse, L., Clerbaux, C., Hermans, C., Lutsch, E., Strong, K., Hannigan, J. W., Nakajima, H., Morino, I., Herrera, B., Stremme, W., Grutter, M., Schaap, M., Wichink Kruit, R. J., Notholt, J., Coheur, P.-F., and Erisman, J. W.: An evaluation of IASI-NH_3 with ground-based Fourier transform infrared spectroscopy measurements, Atmospheric Chemistry and Physics, 16, 10 351–10 368, https://doi.org/10.5194/acp-16-10351-2016, 2016.

Dammers, E., McLinden, C. A., Griffin, D., Shephard, M. W., Van Der Graaf, S., Lutsch, E., Schaap, M., Gainairu-Matz, Y., Fioletov, V., Van Damme, M., Whitburn, S., Clarisse, L., Cady-Pereira, K., Clerbaux, C., Coheur, P. F., and Erisman, J. W.: NH_3 emissions from large point sources derived from CrIS and IASI satellite observations, Atmospheric Chemistry and Physics, 19, 12 261–12 293, https://doi.org/10.5194/acp-19-12261-2019, 2019.

De Mazière, M., Thompson, A. M., Kurylo, M. J., Wild, J. D., Bernhard, G., Blumenstock, T., Braathen, G. O., Hannigan, J. W., Lambert, J.-C., Leblanc, T., McGee, T. J., Nedoluha, G., Petropavlovskikh, I., Seckmeyer, G., Simon, P. C., Steinbrecht, W., and Strahan, S. E.: The Network for the Detection of Atmospheric Composition Change (NDACC): history, status and perspectives, Atmospheric Chemistry and Physics, 18, 4935–4964, https://doi.org/10.5194/acp-18-4935-2018, 2018.

Eastham, S. D., Long, M. S., Keller, C. A., Lundgren, E., Yantosca, R. M., Zhuang, J., Li, C., Lee, C. J., Yannetti, M., Auer, B. M., Clune, T. L., Kouatchou, J., Putman, W. M., Thompson, M. A., Trayanov, A. L., Molod, A. M., Martin, R. V., and Jacob, D. J.: GEOS-Chem High Performance (GCHP v11-02c): a next-generation implementation of the GEOS-Chem chemical transport model for massively parallel applications, Geoscientific Model Development, 11, 2941–2953, https://doi.org/10.5194/gmd-11-2941-2018, 2018.

European Environment Agency: National Emission Reduction Commitments Directive 2023, uRL: https://www.eea.europa.eu/publications/national-emission-reduction-commitments-directive-2023. Last access: February, 2025, 2023.

Evangeliou, N., Balkanski, Y., Eckhardt, S., Cozic, A., Van Damme, M., Coheur, P.-F., Clarisse, L., Shephard, M. W., Cady-Pereira, K. E., and Hauglustaine, D.: 10-year satellite-constrained fluxes of ammonia improve performance of chemistry transport models, Atmospheric Chemistry and Physics, 21, 4431–4451, https://doi.org/10.5194/acp-21-4431-2021, 2021.

Eyring, V., Waugh, D. W., Bodeker, G. E., Cordero, E., Akiyoshi, H., Austin, J., Beagley, S. R., Boville, B. A., Braesicke, P., Brühl, C., Butchart, N., Chipperfield, M. P., Dameris, M., Deckert, R., Deushi, M., Frith, S. M., Garcia, R. R., Gettelman, A., Giorgetta, M. A., Kinnison, D. E., Mancini, E., Manzini, E., Marsh, D. R., Matthes, S., Nagashima, T., Newman, P. A., Nielsen, J. E., Pawson, S., Pitari, G., Plummer, D. A., Rozanov, E., Schraner, M., Scinocca, J. F., Semeniuk, K., Shepherd, T. G., Shibata, K., Steil, B., Stolarski, R. S., Tian,

https://doi.org/10.5194/egusphere-2026-3138
Preprint. Discussion started: 15 June 2026

W., and Yoshiki, M.: Multimodel projections of stratospheric ozone in the 21st century, Journal of Geophysical Research: Atmospheres, 112, https://doi.org/https://doi.org/10.1029/2006JD008332, 2007.

Flood, V. A., Strong, K., Whaley, C. H., Walker, K. A., Blumenstock, T., Hannigan, J. W., Mellqvist, J., Notholt, J., Palm, M., Röhling, A. N., Arnold, S., Beagley, S., Chien, R.-Y., Christensen, J., Deushi, M., Dobricic, S., Dong, X., Fu, J. S., Gauss, M., Gong, W., Langner, J., Law, K. S., Marelle, L., Onishi, T., Oshima, N., Plummer, D. A., Pozzoli, L., Raut, J.-C., Thomas, M. A., Tsyro, S., and Turnock, S.: Evaluating modelled tropospheric columns of CH_4, CO, and O_3 in the Arctic using ground-based Fourier transform infrared (FTIR) measurements, Atmospheric Chemistry and Physics, 24, 1079–1118, https://doi.org/10.5194/acp-24-1079-2024, 2024.

Fowler, D., Coyle, M., Skiba, U., Sutton, M. A., Cape, J. N., Reis, S., Sheppard, L. J., Jenkins, A., Grizzetti, B., Galloway, J. N., Vitousek, P., Leach, A., Bouwman, A. F., Butterbach-Bahl, K., Dentener, F., Stevenson, D., Amann, M., and Voss, M.: The global nitrogen cycle in the twenty-first century, Philosophical Transactions of the Royal Society B: Biological Sciences, 368, 20130 164, https://doi.org/10.1098/rstb.2013.0164, 2013.

Franco, B., Marais, E. A., Bovy, B., Bader, W., Lejeune, B., Roland, G., Servais, C., and Mahieu, E.: Diurnal cycle and multi-decadal trend of formaldehyde in the remote atmosphere near 46° N, Atmospheric Chemistry and Physics, 16, 4171–4189, https://doi.org/10.5194/acp-16-4171-2016, 2016.

Friedrich, M., Beutner, E., Reuvers, H., Smeekes, S., Urbain, J.-P., Bader, W., Franco, B., Lejeune, B., and Mahieu, E.: A statistical analysis of time trends in atmospheric ethane, Climatic Change, 162, 105–125, https://doi.org/10.1007/s10584-020-02806-2, 2020.

García, O. E., Schneider, M., Sepúlveda, E., Hase, F., Blumenstock, T., Cuevas, E., Ramos, R., Gross, J., Barthlott, S., Röhling, A. N., Sanromá, E., González, Y., Gómez-Peláez, A. J., Navarro-Comas, M., Puentedura, O., Yela, M., Redondas, A., Carreño, V., León-Luis, S. F., Reyes, E., García, R. D., Rivas, P. P., Romero-Campos, P. M., Torres, C., Prats, N., Hernández, M., and López, C.: Twenty years of ground-based NDACC FTIR spectrometry at Izaña Observatory – overview and long-term comparison to other techniques, Atmospheric Chemistry and Physics, 21, 15 519–15 554, https://doi.org/10.5194/acp-21-15519-2021, 2021.

García, R. D., García, O. E., Cuevas-Agulló, E., Barreto, Á., Cachorro, V. E., Marrero, C., Almansa, F., Ramos, R., and Pó, M.: Spectral Aerosol Radiative Forcing and Efficiency of the La Palma Volcanic Plume over the Izaña Observatory, Remote Sensing, 15, https://doi.org/10.3390/rs15010173, 2023.

Gardiner, T., Forbes, A., de Mazière, M., Vigouroux, C., Mahieu, E., Demoulin, P., Velazco, V., Notholt, J., Blumenstock, T., Hase, F., Kramer, I., Sussmann, R., Stremme, W., Mellqvist, J., Strandberg, A., Ellingsen, K., and Gauss, M.: Trend analysis of greenhouse gases over Europe measured by a network of ground-based remote FTIR instruments, Atmospheric Chemistry and Physics, 8, 6719–6727, https://doi.org/10.5194/acp-8-6719-2008, 2008.

Gelaro, R., McCarty, W., Suárez, M. J., Todling, R., Molod, A., Takacs, L., Randles, C. A., Darmenov, A., Bosilovich, M. G., Reichle, R., Wargan, K., Coy, L., Cullather, R., Draper, C., Akella, S., Buchard, V., Conaty, A., Da Silva, A. M., Gu, W., Kim, G.-K., Koster, R., Lucchesi, R., Merkova, D., Nielsen, J. E., Partyka, G., Pawson, S., Putman, W., Rienecker, M., Schubert, S. D., Sienkiewicz, M., and Zhao, B.: The Modern-Era Retrospective Analysis for Research and Applications, Version 2 (MERRA-2), Journal of Climate, 30, 5419–5454, https://doi.org/10.1175/jcli-d-16-0758.1, 2017.

GEOS-Chem: GEOS-Chem High Performance (Version 14.1.0), uRL: https://zenodo.org/records/7600586. Last access: February, 2024, 2023.

Giannakis, E., Kushta, J., Bruggeman, A., and Lelieveld, J.: Costs and benefits of agricultural ammonia emission abatement options for compliance with European air quality regulations, Environmental Sciences Europe, 31, 93, https://doi.org/10.1186/s12302-019-0275-0, 2019.

https://doi.org/10.5194/egusphere-2026-3138
Preprint. Discussion started: 15 June 2026

Government of Canada: Air Pollutant Emissions, uRL: https://www.canada.ca/en/environment-climate-change/services/environmental-indicators/air-pollutant-emissions.html. Last access: February, 2025, 2023.

Graedel, T. E., Bates, T. S., Bouwman, A. F., Cunnold, D., Dignon, J., Fung, I., Jacob, D. J., Lamb, B. K., Logan, J. A., Marland, G., Middleton, P., Pacyna, J. M., and Placet, M.and Veldt, C.: A compilation of inventories of emissions to the atmosphere, Global Biogeochemical Cycles, pp. 1 – 26, https://doi.org/https://doi.org/10.1029/92GB02793, 1993.

Gu, M., Pan, Y., Walters, W. W., Sun, Q., Song, L., Wang, Y., Xue, Y., and Fang, Y.: Vehicular Emissions Enhanced Ammonia Concentrations in Winter Mornings: Insights from Diurnal Nitrogen Isotopic Signatures, Environmental Science & Technology, 56, 1578–1585, https://doi.org/10.1021/acs.est.1c05884, pMID: 35050606, 2022.

Hase, F., Hannigan, J., Coffey, M., Goldman, A., Höpfner, M., Jones, N., Rinsland, C., and Wood, S.: Intercomparison of retrieval codes used for the analysis of high-resolution, ground-based FTIR measurements, Journal of Quantitative Spectroscopy and Radiative Transfer, 87, 25–52, https://doi.org/10.1016/j.jqsrt.2003.12.008, 2004.

Herrera, B., Bezanilla, A., Blumenstock, T., Dammers, E., Hase, F., Clarisse, L., Magaldi, A., Rivera, C., Stremme, W., Strong, K., Viatte, C., Van Damme, M., and Grutter, M.: Measurement report: Evolution and distribution of NH_3 over Mexico City from ground-based and satellite infrared spectroscopic measurements, Atmospheric Chemistry and Physics, 22, 14 119–14 132, https://doi.org/10.5194/acp-22-14119-2022, 2022.

Herrera Gutierrez, B., Dammers, E., Maziere, M. D., Garcia, O., Grutter, M., Hannigan, J. W., Jones, N., Mahieu, E., Makarova, M., Morino, I., Murata, I., Ortega, I., Palm, M., Poverovskii, A., Smale, D., Stremme, W., Sussmann, R., Toon, G., Vigouroux, C., Wang, W., Wizenberg, T., and Strong, K.: Replication Data for: Ammonia variability and trends from globally distributed FTIR measurements and model simulations, https://doi.org/10.5683/SP3/9UV6KA, 2025.

Hoesly, R. M., Smith, S. J., Feng, L., Klimont, Z., Janssens-Maenhout, G., Pitkanen, T., Seibert, J. J., Vu, L., Andres, R. J., Bolt, R. M., Bond, T. C., Dawidowski, L., Kholod, N., Kurokawa, J.-I., Li, M., Liu, L., Lu, Z., Moura, M. C. P., O'Rourke, P. R., and Zhang, Q.: Historical (1750–2014) anthropogenic emissions of reactive gases and aerosols from the Community Emissions Data System (CEDS), Geoscientific Model Development, 11, 369–408, https://doi.org/10.5194/gmd-11-369-2018, 2018.

Huijnen, V., Miyazaki, K., Flemming, J., Inness, A., Sekiya, T., and Schultz, M. G.: An intercomparison of tropospheric ozone reanalysis products from CAMS, CAMS interim, TCR-1, and TCR-2, Geoscientific Model Development, 13, 1513–1544, https://doi.org/10.5194/gmd-13-1513-2020, 2020.

Janssens-Maenhout, G., Crippa, M., Guizzardi, D., Dentener, F., Muntean, M., Pouliot, G., Keating, T., Zhang, Q., Kurokawa, J., Wankmüller, R., Denier van der Gon, H., Kuenen, J. J. P., Klimont, Z., Frost, G., Darras, S., Koffi, B., and Li, M.: HTAP v2.2: a mosaic of regional and global emission grid maps for 2008 and 2010 to study hemispheric transport of air pollution, Atmospheric Chemistry and Physics, 15, 11 411–11 432, https://doi.org/10.5194/acp-15-11411-2015, 2015.

Jarvis, S. and Ledgard, S.: Ammonia emissions from intensive dairying: a comparison of contrasting systems in the United Kingdom and New Zealand, Agriculture, Ecosystems & Environment, 92, 83–92, https://doi.org/https://doi.org/10.1016/S0167-8809(01)00283-3, 2002.

Kaiser, J. W., Heil, A., Andreae, M. O., Benedetti, A., Chubarova, N., Jones, L., Morcrette, J.-J., Razinger, M., Schultz, M. G., Suttie, M., and van der Werf, G. R.: Biomass burning emissions estimated with a global fire assimilation system based on observed fire radiative power, Biogeosciences, 9, 527–554, https://doi.org/10.5194/bg-9-527-2012, 2012.

Keeley, J. E. and Syphard, A. D.: Large California wildfires: 2020 fires in historical context, Fire Ecology, 17, https://doi.org/10.1186/s42408-021-00110-7, 2021.

https://doi.org/10.5194/egusphere-2026-3138
Preprint. Discussion started: 15 June 2026

Khan, M., Lowe, D., Derwent, R., Foulds, A., Chhantyal-Pun, R., McFiggans, G., Orr-Ewing, A., Percival, C., and Shallcross, D.: Global and regional model simulations of atmospheric ammonia, Atmospheric Research, 234, 104 702, https://doi.org/10.1016/j.atmosres.2019.104702, 2020.

Kotnala, G., Sharma, S., and Mandal, T. K.: Influence of Vehicular Emissions (NO, NO_2, CO and NMHCs) on the Mixing Ratio of Atmospheric Ammonia (NH_3) in Delhi, India, Archives of Environmental Contamination and Toxicology, 78, 79–85, https://doi.org/https://doi.org/10.1007/s00244-019-00689-8, 2019.

Kutzner, R. D., Cuesta, J., Chelin, P., Petit, J.-E., Ray, M., Landsheere, X., Tournadre, B., Dupont, J.-C., Rosso, A., Hase, F., Orphal, J., and Beekmann, M.: Diurnal evolution of total column and surface atmospheric ammonia in the megacity of Paris, France, during an intense springtime pollution episode, Atmospheric Chemistry and Physics, 21, 12 091–12 111, https://doi.org/10.5194/acp-21-12091-2021, 2021.

Kärnä, T. and Baptista, A. M.: Evaluation of a long-term hindcast simulation for the Columbia River estuary, Ocean Modelling, 99, 1–14, https://doi.org/https://doi.org/10.1016/j.ocemod.2015.12.007, 2016.

Laughner, J. L., Toon, G. C., Mendonca, J., Petri, C., Roche, S., Wunch, D., Blavier, J.-F., Griffith, D. W. T., Heikkinen, P., Keeling, R. F., Kiel, M., Kivi, R., Roehl, C. M., Stephens, B. B., Baier, B. C., Chen, H., Choi, Y., Deutscher, N. M., DiGangi, J. P., Gross, J., Herkommer, B., Jeseck, P., Laemmel, T., Lan, X., McGee, E., McKain, K., Miller, J., Morino, I., Notholt, J., Ohyama, H., Pollard, D. F., Rettinger, M., Riris, H., Rousogenous, C., Sha, M. K., Shiomi, K., Strong, K., Sussmann, R., Té, Y., Velazco, V. A., Wofsy, S. C., Zhou, M., and Wennberg, P. O.: The Total Carbon Column Observing Network's GGG2020 data version, Earth System Science Data, 16, 2197–2260, https://doi.org/10.5194/essd-16-2197-2024, 2024.

Lutsch, E., Strong, K., Jones, D. B., Ortega, I., Hannigan, J. W., Dammers, E., Shephard, M. W., Morris, E., Murphy, K., Evans, M. J., Parrington, M., Whitburn, S., Van Damme, M., Clarisse, L., Coheur, P. F., Clerbaux, C., Croft, B., Martin, R. V., Pierce, J. R., and Fisher, J. A.: Unprecedented Atmospheric Ammonia Concentrations Detected in the High Arctic From the 2017 Canadian Wildfires, Journal of Geophysical Research: Atmospheres, 124, 8178–8202, https://doi.org/10.1029/2019JD030419, 2019.

Marsh, D. R., Mills, M. J., Kinnison, D. E., Lamarque, J.-F., Calvo, N., and Polvani, L. M.: Climate Change from 1850 to 2005 Simulated in CESM1(WACCM), Journal of Climate, 26, 7372 – 7391, https://doi.org/10.1175/JCLI-D-12-00558.1, 2013.

Martin, R. V., Eastham, S. D., Bindle, L., Lundgren, E. W., Clune, T. L., Keller, C. A., Downs, W., Zhang, D., Lucchesi, R. A., Sulprizio, M. P., Yantosca, R. M., Li, Y., Estrada, L., Putman, W. M., Auer, B. M., Trayanov, A. L., Pawson, S., and Jacob, D. J.: Improved advection, resolution, performance, and community access in the new generation (version 13) of the high-performance GEOS-Chem global atmospheric chemistry model (GCHP), Geoscientific Model Development, 15, 8731–8748, https://doi.org/10.5194/gmd-15-8731-2022, 2022.

Miyazaki, K., Eskes, H. J., Sudo, K., Takigawa, M., van Weele, M., and Boersma, K. F.: Simultaneous assimilation of satellite NO_2, O_3, CO, and HNO_3 data for the analysis of tropospheric chemical composition and emissions, Atmospheric Chemistry and Physics, 12, 9545–9579, https://doi.org/10.5194/acp-12-9545-2012, 2012.

Miyazaki, K., Eskes, H. J., and Sudo, K.: A tropospheric chemistry reanalysis for the years 2005–2012 based on an assimilation of OMI, MLS, TES, and MOPITT satellite data, Atmospheric Chemistry and Physics, 15, 8315–8348, https://doi.org/10.5194/acp-15-8315-2015, 2015.

Miyazaki, K., Bowman, K., Sekiya, T., Eskes, H., Boersma, F., Worden, H., Livesey, N., Payne, V. H., Sudo, K., Kanaya, Y., Takigawa, M., and Ogochi, K.: Chemical Reanalysis Products, https://doi.org/10.25966/9qgv-fe81, 2019.

https://doi.org/10.5194/egusphere-2026-3138
Preprint. Discussion started: 15 June 2026

Miyazaki, K., Bowman, K. W., Sekiya, T., Eskes, H., Boersma, F., Worden, H., Livesey, N., Payne, V. H., Sudo, K., Kanaya, Y., Takigawa, M., and Ogochi, K.: Updated tropospheric chemistry reanalysis and emission estimates, TCR-2, for 2005–2018, Earth System Science Data, 12, 2223–2259, https://doi.org/10.5194/essd-12-2223-2020, 2020a.

Miyazaki, K., Bowman, K. W., Yumimoto, K., Walker, T., and Sudo, K.: Evaluation of a multi-model, multi-constituent assimilation framework for tropospheric chemical reanalysis, Atmospheric Chemistry and Physics, 20, 931–967, https://doi.org/10.5194/acp-20-931-2020, 2020b.

Murphy, J. G., Wentworth, G. R., Moravek, A., Collins, D. B., and Sharma, S.: Processes regulating the sources and sinks of ammonia in the Canadian Arctic, Faraday Discuss., https://doi.org/10.1039/D4FD00173G, 2025.

Nair, A. A. and Yu, F.: Quantification of Atmospheric Ammonia Concentrations: A Review of Its Measurement and Modeling, Atmosphere, 11, 1092, https://doi.org/10.3390/atmos11101092, 2020.

Olabi, A., Abdelkareem, M. A., Al-Murisi, M., Shehata, N., Alami, A. H., Radwan, A., Wilberforce, T., Chae, K.-J., and Sayed, E. T.: Recent progress in Green Ammonia: Production, applications, assessment; barriers, and its role in achieving the sustainable development goals, Energy Conversion and Management, 277, 116 594, https://doi.org/10.1016/j.enconman.2022.116594, 2023.

Osada, K., Saito, S., Tsurumaru, H., and Hoshi, J.: Vehicular exhaust contributions to high NH_3 and $PM_{2.5}$ concentrations during winter in Tokyo, Japan, Atmospheric Environment, 206, 218–224, https://doi.org/https://doi.org/10.1016/j.atmosenv.2019.03.008, 2019.

Paleczny, M., Hammill, E., Karpouzi, V., and Pauly, D.: Population Trend of the World's Monitored Seabirds, 1950-2010, PLOS ONE, 10, 1–11, https://doi.org/10.1371/journal.pone.0129342, 2015.

Pan, B., Lam, S. K., Mosier, A., Luo, Y., and Deli, C.: Strategies for mitigating ammonia emissions from agroecosystems, In Proceedings of the 2016 International Nitrogen Initiative Conference. URL: https://agronomyaustraliaproceedings.org/images/sampledata/ini2016/pdf-papers/INI2016_Pan_Baobao.pdf. Last access: February, 2025, 2016.

Panchasara, H., Samrat, N. H., and Islam, N.: Greenhouse Gas Emissions Trends and Mitigation Measures in Australian Agriculture Sector A Review, Agriculture, 11, https://doi.org/10.3390/agriculture11020085, 2021.

Pannell, D. and Rogers, A.: Agriculture and the Environment: Policy Approaches in Australia and New Zealand, Review of Environmental Economics and Policy, 16, 126–145, https://doi.org/10.1086/718053, 2022.

Parfitt, R. L., Baisden, W. T., Schipper, L. A., and and, A. D. M.: Nitrogen inputs and outputs for New Zealand at national and regional scales: past, present and future scenarios, Journal of the Royal Society of New Zealand, 38, 71–87, https://doi.org/10.1080/03014220809510547, 2008.

Paulot, F., Jacob, D. J., Pinder, R. W., Bash, J. O., Travis, K., and Henze, D. K.: Ammonia emissions in the United States, European Union, and China derived by high-resolution inversion of ammonium wet deposition data: Interpretation with a new agricultural emissions inventory (MASAGE_NH_3), Journal of Geophysical Research: Atmospheres, 119, 4343–4364, https://doi.org/10.1002/2013JD021130, 2014.

Philip, S., Martin, R. V., and Keller, C. A.: Sensitivity of chemistry-transport model simulations to the duration of chemical and transport operators: A case study with GEOS-chem V10-01, Geoscientific Model Development, 9, 1683–1695, https://doi.org/10.5194/gmd-9-1683-2016, 2016.

Prignon, M., Chabrillat, S., Minganti, D., O'Doherty, S., Servais, C., Stiller, G., Toon, G. C., Vollmer, M. K., and Mahieu, E.: Improved FTIR retrieval strategy for HCFC-22 (CHClF2), comparisons with in situ and satellite datasets with the support of models, and determination of its long-term trend above Jungfraujoch, Atmospheric Chemistry and Physics, 19, 12 309–12 324, https://doi.org/10.5194/acp-19-12309-2019, 2019.

https://doi.org/10.5194/egusphere-2026-3138
Preprint. Discussion started: 15 June 2026

Pye, H. O. T., Nenes, A., Alexander, B., Ault, A. P., Barth, M. C., Clegg, S. L., Collett Jr., J. L., Fahey, K. M., Hennigan, C. J., Herrmann, H., Kanakidou, M., Kelly, J. T., Ku, I.-T., McNeill, V. F., Riemer, N., Schaefer, T., Shi, G., Tilgner, A., Walker, J. T., Wang, T., Weber, R., Xing, J., Zaveri, R. A., and Zuend, A.: The acidity of atmospheric particles and clouds, Atmospheric Chemistry and Physics, 20, 4809–4888, https://doi.org/10.5194/acp-20-4809-2020, 2020.

Randerson, J., Van Der Werf, G., Giglio, L., Collatz, G., and Kasibhatla, P.: Global Fire Emissions Database, Version 4.1 (GFEDv4), https://doi.org/10.3334/ORNLDAAC/1293, 2017.

Riddick, S., Dragosits, U., Blackall, T., Daunt, F., Wanless, S., and Sutton, M.: The global distribution of ammonia emissions from seabird colonies, Atmospheric Environment, 55, 319–327, https://doi.org/https://doi.org/10.1016/j.atmosenv.2012.02.052, 2012.

Rios, B., Díaz-Esteban, Y., and Raga, G. B.: Smoke emissions from biomass burning in Central Mexico and their impact on air quality in Mexico City: May 2019 case study, Science of The Total Environment, 904, 166 912, https://doi.org/https://doi.org/10.1016/j.scitotenv.2023.166912, 2023.

Roche, S., Strong, K., Wunch, D., Mendonca, J., Sweeney, C., Baier, B., Biraud, S. C., Laughner, J. L., Toon, G. C., and Connor, B. J.: Retrieval of atmospheric CO_2 vertical profiles from ground-based near-infrared spectra, Atmospheric Measurement Techniques, 14, 3087–3118, https://doi.org/10.5194/amt-14-3087-2021, 2021.

Rodgers, C. D. and Connor, B. J.: Intercomparison of remote sounding instruments, Journal of Geophysical Research: Atmospheres, 108, 4116, https://doi.org/https://doi.org/10.1029/2002JD002299, 2003.

Rothman, L., Gordon, I., Barbe, A., Benner, D., Bernath, P., Birk, M., Boudon, V., Brown, L., Campargue, A., Champion, J.-P., Chance, K., Coudert, L., Dana, V., Devi, V., Fally, S., Flaud, J.-M., Gamache, R., Goldman, A., Jacquemart, D., Kleiner, I., Lacome, N., Lafferty, W., Mandin, J.-Y., Massie, S., Mikhailenko, S., Miller, C., Moazzen-Ahmadi, N., Naumenko, O., Nikitin, A., Orphal, J., Perevalov, V., Perrin, A., Predoi-Cross, A., Rinsland, C., Rotger, M., Šimečková, M., Smith, M., Sung, K., Tashkun, S., Tennyson, J., Toth, R., Vandaele, A., and Vander Auwera, J.: The HITRAN 2008 molecular spectroscopic database, Journal of Quantitative Spectroscopy and Radiative Transfer, 110, 533–572, https://doi.org/https://doi.org/10.1016/j.jqsrt.2009.02.013, hITRAN, 2009.

Rothman, L., Gordon, I., Babikov, Y., Barbe, A., Chris Benner, D., Bernath, P., Birk, M., Bizzocchi, L., Boudon, V., Brown, L., Campargue, A., Chance, K., Cohen, E., Coudert, L., Devi, V., Drouin, B., Fayt, A., Flaud, J.-M., Gamache, R., Harrison, J., Hartmann, J.-M., Hill, C., Hodges, J., Jacquemart, D., Jolly, A., Lamouroux, J., Le Roy, R., Li, G., Long, D., Lyulin, O., Mackie, C., Massie, S., Mikhailenko, S., Müller, H., Naumenko, O., Nikitin, A., Orphal, J., Perevalov, V., Perrin, A., Polovtseva, E., Richard, C., Smith, M., Starikova, E., Sung, K., Tashkun, S., Tennyson, J., Toon, G., Tyuterev, V., and Wagner, G.: The HITRAN 2012 molecular spectroscopic database, Journal of Quantitative Spectroscopy and Radiative Transfer, 130, 4–50, https://doi.org/https://doi.org/10.1016/j.jqsrt.2013.07.002, hITRAN2012 special issue, 2013.

Safford, H. D., Paulson, A. K., Steel, Z. L., Young, D. J. N., and Wayman, R. B.: The 2020 California fire season: A year like no other, a return to the past or a harbinger of the future?, Global Ecology and Biogeography, 31, 2005–2025, https://doi.org/https://doi.org/10.1111/geb.13498, 2022.

Saggar, S., Singh, J., Giltrap, D., Zaman, M., Luo, J., Rollo, M., Kim, D.-G., Rys, G., and van der Weerden, T.: Quantification of reductions in ammonia emissions from fertiliser urea and animal urine in grazed pastures with urease inhibitors for agriculture inventory: New Zealand as a case study, Science of The Total Environment, 465, 136–146, https://doi.org/https://doi.org/10.1016/j.scitotenv.2012.07.088, 2013.

Santamarta Cerezal, J., ed.: Avances en la investigación de los recursos hídricos en islas y terrenos volcánicos, Universidad de La Laguna, reunión científica nacional sobre el estudio de los recursos hídricos en islas volcánicas, Nov 2012, Tenerife, 2013.

https://doi.org/10.5194/egusphere-2026-3138
Preprint. Discussion started: 15 June 2026

Sekiya, T., Miyazaki, K., Eskes, H., Bowman, K., Sudo, K., Kanaya, Y., and Takigawa, M.: The worldwide COVID-19 lockdown impacts on global secondary inorganic aerosols and radiative budget, Science Advances, 9, eadh2688, https://doi.org/10.1126/sciadv.adh2688, 2023.

Sen, B., Toon, G. C., Blavier, J.-F., Fleming, E. L., and Jackman, C. H.: Balloon-borne observations of midlatitude fluorine abundance, Journal of Geophysical Research, 101, 9045–9054, https://doi.org/https://10.1029/95JD03440, 1996.

Shephard, M. W. and Cady-Pereira, K. E.: Cross-track Infrared Sounder (CrIS) satellite observations of tropospheric ammonia, Atmospheric Measurement Techniques, 8, 1323–1336, https://doi.org/10.5194/amt-8-1323-2015, 2015.

Shephard, M. W., Cady-Pereira, K. E., Luo, M., Henze, D. K., Pinder, R. W., Walker, J. T., Rinsland, C. P., Bash, J. O., Zhu, L., Payne, V. H., and Clarisse, L.: TES ammonia retrieval strategy and global observations of the spatial and seasonal variability of ammonia, Atmospheric Chemistry and Physics, 11, 10 743–10 763, https://doi.org/10.5194/acp-11-10743-2011, 2011.

Sutton, M. A., Erisman, J. W., Dentener, F., and Möller, D.: Ammonia in the environment: From ancient times to the present, Environmental Pollution, 156, 583–604, https://doi.org/10.1016/j.envpol.2008.03.013, 2008.

Sutton, M. A., Reis, S., Riddick, S. N., Dragosits, U., Nemitz, E., Theobald, M. R., Tang, Y. S., Braban, C. F., Vieno, M., Dore, A. J., Mitchell, R. F., Wanless, S., Daunt, F., Fowler, D., Blackall, T. D., Milford, C., Flechard, C. R., Loubet, B., Massad, R., Cellier, P., Personne, E., Coheur, P. F., Clarisse, L., Van Damme, M., Ngadi, Y., Clerbaux, C., Skjøth, C. A., Geels, C., Hertel, O., Wichink Kruit, R. J., Pinder, R. W., Bash, J. O., Walker, J. T., Simpson, D., Horváth, L., Misselbrook, T. H., Bleeker, A., Dentener, F., and De Vries, W.: Towards a climate-dependent paradigm of ammonia emission and deposition, Philosophical Transactions of the Royal Society B: Biological Sciences, 368, 20130 166, https://doi.org/10.1098/rstb.2013.0166, 2013.

Tan, J., Fu, J. S., and Seinfeld, J. H.: Ammonia emission abatement does not fully control reduced forms of nitrogen deposition, Proceedings of the National Academy of Sciences, 117, 9771–9775, https://doi.org/10.1073/pnas.1920068117, 2020.

Tichý, O., Eckhardt, S., Balkanski, Y., Hauglustaine, D., and Evangeliou, N.: Decreasing trends of ammonia emissions over Europe seen from remote sensing and inverse modelling, Atmospheric Chemistry and Physics, 23, 15 235–15 252, https://doi.org/10.5194/acp-23-15235-2023, 2023.

Toon, G. C.: The JPL MkIV Interferometer, Optics and Photonics News, 2, 19–21, 1991.

Toon, G. C., Blavier, J.-F. L., and Sung, K.: Measurements of atmospheric ethene by solar absorption FTIR spectrometry, Atmospheric Chemistry and Physics, 18, 5075–5088, https://doi.org/10.5194/acp-18-5075-2018, 2018.

Uematsu, M., Toratani, M., Kajino, M., Narita, Y., Senga, Y., and Kimoto, T.: Enhancement of primary productivity in the Western North Pacific caused by the eruption of the Miyake-Jima Volcano, Geophysical Research Letters, 31, https://doi.org/10.1029/2003GL018790, 2004.

U.S. Environmental Protection Agency: Acid Rain Program Results, uRL: https://www.epa.gov/acidrain/acid-rain-program-results. Last access: February, 2025, 2024.

Van Damme, M., Erisman, J. W., Clarisse, L., Dammers, E., Whitburn, S., Clerbaux, C., Dolman, A. J., and Coheur, P.-F.: Worldwide spatiotemporal atmospheric ammonia (NH_3) columns variability revealed by satellite, Geophysical Research Letters, 42, 8660–8668, https://doi.org/10.1002/2015GL065496, 2015.

Van Damme, M., Clarisse, L., Franco, B., Sutton, M. A., Erisman, J. W., Wichink Kruit, R., van Zanten, M., Whitburn, S., Hadji-Lazaro, J., Hurtmans, D., Clerbaux, C., and Coheur, P.-F.: Global, regional and national trends of atmospheric ammonia derived from a decadal (2008–2018) satellite record, Environmental Research Letters, 16, 055 017, https://doi.org/10.1088/1748-9326/abd5e0, 2021.

Varotsos, C., Ondov, J., and Efstathiou, M.: Scaling properties of air pollution in Athens, Greece and Baltimore, Maryland, Atmospheric Environment, 39, 4041–4047, https://doi.org/10.1016/j.atmosenv.2005.03.024, 2005.

https://doi.org/10.5194/egusphere-2026-3138
Preprint. Discussion started: 15 June 2026

Viatte, C., Wang, T., Van Damme, M., Dammers, E., Meleux, F., Clarisse, L., Shephard, M. W., Whitburn, S., Coheur, P. F., Cady-Pereira, K. E., and Clerbaux, C.: Atmospheric ammonia variability and link with particulate matter formation: a case study over the Paris area, Atmospheric Chemistry and Physics, 20, 577–596, https://doi.org/10.5194/acp-20-577-2020, 2020.

Viatte, C., Guendouz, N., Dufaux, C., Hensen, A., Swart, D., Van Damme, M., Clarisse, L., Coheur, P., and Clerbaux, C.: Measurement report: Ammonia in Paris derived from ground-based open-path and satellite observations, Atmospheric Chemistry and Physics, 23, 15 253–15 267, https://doi.org/10.5194/acp-23-15253-2023, 2023.

Vigouroux, C., Blumenstock, T., Coffey, M., Errera, Q., García, O., Jones, N. B., Hannigan, J. W., Hase, F., Liley, B., Mahieu, E., Mellqvist, J., Notholt, J., Palm, M., Persson, G., Schneider, M., Servais, C., Smale, D., Thölix, L., and De Mazière, M.: Trends of ozone total columns and vertical distribution from FTIR observations at eight NDACC stations around the globe, Atmospheric Chemistry and Physics, 15, 2915–2933, https://doi.org/10.5194/acp-15-2915-2015, 2015.

Warner, J. X., Dickerson, R. R., Wei, Z., Strow, L. L., Wang, Y., and Liang, Q.: Increased atmospheric ammonia over the world's major agricultural areas detected from space, Geophysical Research Letters, 44, 2875–2884, https://doi.org/10.1002/2016GL072305, 2017.

Watanabe, S., Hajima, T., Sudo, K., Nagashima, T., Takemura, T., Okajima, H., Nozawa, T., Kawase, H., Abe, M., Yokohata, T., Ise, T., Sato, H., Kato, E., Takata, K., Emori, S., and Kawamiya, M.: MIROC-ESM 2010: model description and basic results of CMIP5-20c3m experiments, Geoscientific Model Development, 4, 845–872, https://doi.org/10.5194/gmd-4-845-2011, 2011.

Wentworth, G. R., Murphy, J. G., Croft, B., Martin, R. V., Pierce, J. R., Côté, J.-S., Courchesne, I., Tremblay, J.-É., Gagnon, J., Thomas, J. L., Sharma, S., Toom-Sauntry, D., Chivulescu, A., Levasseur, M., and Abbatt, J. P. D.: Ammonia in the summertime Arctic marine boundary layer: sources, sinks, and implications, Atmospheric Chemistry and Physics, 16, 1937–1953, https://doi.org/10.5194/acp-16-1937-2016, 2016.

Whitburn, S., Van Damme, M., Kaiser, J., Van Der Werf, G., Turquety, S., Hurtmans, D., Clarisse, L., Clerbaux, C., and Coheur, P.-F.: Ammonia emissions in tropical biomass burning regions: Comparison between satellite-derived emissions and bottom-up fire inventories, Atmospheric Environment, 121, 42–54, https://doi.org/10.1016/j.atmosenv.2015.03.015, 2015.

Whitburn, S., Van Damme, M., Clarisse, L., Hurtmans, D., Clerbaux, C., and Coheur, P.-F.: IASI-derived NH_3 enhancement ratios relative to CO for the tropical biomass burning regions, Atmospheric Chemistry and Physics, 17, 12 239–12 252, https://doi.org/10.5194/acp-17-12239-2017, 2017.

Wizenberg, T., Strong, K., Jones, D. B. A., Hannigan, J. W., Ortega, I., and Mahieu, E.: Measured and Modeled Trends of Seven Tropospheric Pollutants in the High Arctic From 1999 to 2022, Journal of Geophysical Research: Atmospheres, 129, e2023JD040 544, https://doi.org/https://doi.org/10.1029/2023JD040544, e2023JD040544 2023JD040544, 2024.

Yamanouchi, S., Viatte, C., Strong, K., Lutsch, E., Jones, D. B. A., Clerbaux, C., Van Damme, M., Clarisse, L., and Coheur, P.-F.: Multiscale observations of NH_3 around Toronto, Canada, Atmospheric Measurement Techniques, 14, 905–921, https://doi.org/10.5194/amt-14-905-2021, 2021.

Yao, X. and Zhang, L.: Trends in atmospheric ammonia at urban, rural, and remote sites across North America, Atmospheric Chemistry and Physics, 16, 11 465–11 475, https://doi.org/10.5194/acp-16-11465-2016, 2016.

Zeng, Z.-C., Natraj, V., Xu, F., Chen, S., Gong, F.-Y., Pongetti, T. J., Sung, K., Toon, G., Sander, S. P., and Yung, Y. L.: GFIT3: A full physics retrieval algorithm for remote sensing of greenhouse gases in the presence of aerosols, Atmospheric Measurement Techniques, 14, 6483–6507, https://doi.org/10.5194/amt-14-6483-2021, 2021.

Zhang, X., Sun, Y., Liang, X., Lam, S. K., Liu, L., Gu, B., and Chen, D.: Costs and benefits of ammonia abatement in Australia, Resources, Conservation and Recycling, 182, 106 318, https://doi.org/https://doi.org/10.1016/j.resconrec.2022.106318, 2022.

https://doi.org/10.5194/egusphere-2026-3138
Preprint. Discussion started: 15 June 2026

Zhu, L., Henze, D., Bash, J., Jeong, G.-R., Cady-Pereira, K., Shephard, M., Luo, M., Paulot, F., and Capps, S.: Global evaluation of
865 ammonia bidirectional exchange and livestock diurnal variation schemes, Atmospheric Chemistry and Physics, 15, 12 823–12 843, https://doi.org/10.5194/acp-15-12823-2015, 2015.